

Three-Dimensional Collision Avoidance Control for UAVs using Kinematic-based Collision Threat Situation Modeling Approach

Tata Sudyanto^{1,2}, Bambang Riyanto Trilaksono¹, Agus Budiyo^{2,3}, and
Widyawardhana Adiprawita¹

¹School of Electrical and Informatics Engineering, Institut Teknologi Bandung

²Parametrik Solusi Integrasi, Bandung

³Bhimasena Research and Development Center, Bandung

Abstract: Two approaches of collision avoidance (CA) control design are discussed: the stochastic process -based CA and the reactive CA. We believe that the well-established stochastic process -based CA that has been widely used in general aviation flights may not work well in UAV flights for at least two reasons: the difference in encounter characteristics, and the difference in available resource provisions. Problems on reactive CA and search-based CA are mostly simplified to two-dimensional flight cases and depend heavily on non-partisan observer in providing motion data to the onboard controller, thus resulting CA control systems that are ever-dependent to external sensory resources. This shortcoming can potentially be solved using kinematic-based collision threat situation (CTS) model. Existing CTS models using ‘collision cone’ or velocity obstacle (VO) approach are discussed. These models reveal the existence of an infinite number of evasion planes for a given initial threat situation, which requires the CA controller using such approach to search for a plane that provides the most efficient evasive maneuver, which in turn requires more computing power and time. To overcome these shortcomings, we propose a CTS model that is based on the kinematic relation between pair of bodies involved in a CTS. We also define the state of the CTS model and construct the CA controller to reduce the value of the state of the CTS. Since the CTS is evaluated in relative motion context between the bodies, the resulting model is readily compatible with output data from onboard sensors, eliminating the need to perform coordinate transformation that will in turn improving the computational efficiency of the whole CA control system. Furthermore, the model also provides us a deterministic evasion plane, thus eliminating the need to perform a search procedure. The performance of our CA control design is evaluated using energy-based function and a series of simulations.

Keyphrases: Collision avoidance (CA), kinematics, collision threat situation (CTS), gyroscopic action, UAV

1. Introduction

Collision is a condition where two bodies occupy the same region in physical space at the same time. In reality, such condition never actually occurs since it is always preceded by an impact that generates a pair of repulsive forces in the direction that generally separates the two bodies. Such repulsive forces, in most cases, have damaging effect on the two bodies involved in that collision. Therefore, the study about collision is important since preventing collision means preventing damage, which in turn, saving cost and even lives. In studies about vehicle control system, collision condition is one of important subjects that must be considered, especially in designing control system for vehicles such as UAVs that will navigate autonomously in environment with many uncertainties. Among other things, such uncertainties may be the number of obstacles, the geometric size of obstacle, the state of motion of the obstacle, whether it is static or moving, how it behaves when it moves, *etcetera*.

A. Collision avoidance in General Aviation vs. UAV flights

In general aviation, research on collision avoidance (CA) problem has become a well-established research field; some lead researches are reported in [15]-[18]. Any identified collision threat situation (CTS) is called a conflict in the sense that the projected position of own aircraft on some time later occupies the same space as the projected position of an intruder aircraft, hence creating a conflict. Conflict resolving actions are therefore executed to enforce a safe separation distance between the two aircrafts. The conflict resolving action is determined by following the sense-and-avoid principle, which is mostly derived from the see-and-avoid principle in visual flight rule. However, CA problem in general aviation is characterized by long-range encounter and high-speed motion constraint. Long-range encounter allows any detected conflict to be resolved while there is still a large separation distance between conflicting aircrafts. On the other hand, the high-speed motion constraint causes the estimation of conflicting position to be distributed in a large volume region in aerial space. Therefore, CA problem is treated as stochastic process consisting of many interconnected stochastic processes. The interconnection structure is modeled using dynamic Bayesian network structure [14]. More realistic model can be achieved by introducing more relevant parameters followed by providing all necessary equipment to measure the required parameters. Accuracy is maintained to be within the acceptable level due to the cooperative process in the measurement that involves external resources (GPS, intruder aircraft's transponder, and air traffic controller). Researches on collision avoidance control has seen fruitful results in air traffic safety since it has become mandatory that all general aviation aircraft to be equipped with a traffic collision avoidance system (TCAS), a beacon-based collision avoidance system where measurement results about each aircraft's flight condition are shared to other aircrafts via discrete communication [13].

However, the way the CA problem is dealt with in general aviation cannot be necessarily implementable in UAV flights because they are very different in some critical aspects. CA problem in UAV flights involves short-range encounter, which means any collision threat must be avoided as soon as the threat is detected, and with limited possible evasive maneuver. The relatively small dimension leads to many limitations in available resources a UAV system can have on board, including the availability of computing and communication power. A beacon-based cooperative sensor system similar with TCAS will certainly require additional communication resources and may not be feasible to be applied in UAV system. And cooperative measurement from a non-moving platforms, *e.g.*, from a ground station, will definitely limit the UAV's flying coverage. Therefore, a reliable and high speed sensor system, such as lidar-based sensor system, is critical to the CA process. With this regard, a working CA controller in UAV flight is characterized by the reactive response to the collision threat since the controller is practically driven by the sensor measurement.

B. Survey on collision avoidance techniques

CA control system strategies can be distinguished according to how the intruder's motion state is obtained and how it is used. There are basically two strategies of CA control system based on how the intruder's motion state is obtained: by cooperative measurement, and by non-cooperative measurement. The measurement is cooperative if it involves using data measured by resources not belonging to the host UAV system. This extra-vehicular resource can be a GPS network, a ground-based motion trackers, *etc.*, which will defeat the independency of a UAV system in executing collision avoidance autonomously. The data being shared to the host UAV system is typically expressed in a coordinate reference system that is common to both the original observer system and the host UAV system, *e.g.*, the North-East-Down (NED) coordinate system. Consequently, in CA control systems that are based on cooperative measurement, CA control solution is transformed to the host UAV body coordinate system upon implementation. On the other hand, such transformation is not required in CA control systems that are based on non-cooperative measurement because both CA control solution and intruder's motion state already use the same coordinate system. Most published works on CA control design use this approach since CA control problem is always presented and coupled with goal tracking problem.

The intruder's motion state can be used as explicit input to a function or system of functions that ultimately generate the CA control solution. We call such approach as explicit approach, or reactive approach (due to the resulting reactive behavior). Alternatively, the intruder's motion state can also be used to define obstacle, (or forbidden) region in the motion space. Then another algorithm is used to search for a control solution that gives the resulting vehicle's motion leaving the forbidden region. We call such approach as the search approach.

CA control strategy that belongs to reactive CA are potential field (PF) -driven CA. The potential field is a virtual field generated in the vicinity of each intruder's body with its geometric center as the source where the potential value is infinitely high, and the CA controller will maneuver the controlled vehicle along a trajectory with the most negative potential gradient. When multiple intruders present, the resulting potential field is simply the summation of each intruder's. With this regard, PF-driven CA is simple. But the summation may result in one or more location in the field having low potential surrounded by relatively high potential region (local minima) that may trap the controlled vehicle, which is inherent drawback of PF-driven CA. Consequently, a PF-driven CA must rely on other approach to deal with local minima problem. Simpler cases for PF-driven CA are the ones that are designed for controlling holonomic vehicles, and are reported in [1]-[4]. More advance cases involving non-holonomic vehicles (some of vehicle's DOFs are constrained) are reported in [5]-[7].

Kinematic-based CA is another reactive CA strategy that is based on the geometric analysis on intruder's motion state relative to the controlled vehicle. Given an initial vehicle-intruder encounter condition, the analysis can used to determine whether the encounter will lead to a collision or not. If a collision is projected to occur, a collision threat is detected and the CA control solution will then modify the current encounter condition to one that leads to a miss. The kinematic-based CA was contributed and pioneered by Chakravarty & Ghose in 1998 [8]. The main contribution of their work is not exactly the CA control design, but rather the collision threat model they provided, which a CA controller may be based on. The CA controller would work based on the kinematic relation between bodies involved in a collision threat situation. The drawback of this strategy is that all involved geometrical parameters and motion state variables are difficult to obtain by then-available measurement technology.

The search-based CA works by first identifying or searching all possible solution for any given collision threat situation followed by selecting the best (optimal) one of all. The strategy is similar to the path planning procedure with the difference being the characteristics of the environment, which is dynamic, and the length of the finite time horizon, which is much shorter. The path planning procedure regarding collision avoidance is by ensuring the controlled vehicle to follow the planned trajectory that is guaranteed to be collision-free. The main contributor to the development of this strategy are Fiorini and Shiller [9] who developed their CA control design based on a concept of velocity obstacle (VO): a set of all velocity vector in velocity vector space that lead to collision within the time horizon. After a velocity obstacle is identified, a collision-free velocity vector is selected from the set complementary to the velocity obstacle. Fiorini's work also deals with moving obstacles, which modified the original conic-shape velocity obstacle as illustrated in Figure 2 and Figure 3. This strategy was successfully been implemented in planar space with many moving obstacles by Berg *et al* [11], resulting a behavior of a crowd system of autonomous robots that are cooperatively avoiding collision. Jenie, *et al* [12] extended the strategy into the three-dimensional space context and developed a VO-based collision avoidance controller for aerial vehicle flights. Jenie, *et al* also shows the existence of an unlimited number of ways to avoid collision (re-illustrated in Figure 1), from which a working CA controller has to search to obtain an optimal solution. However, the search-based method in calculating CA control solution may not be suitable to UAV system with non-cooperative sensor system since all involved bodies' motion states (the controlled vehicle's and the intruder's) are measured using external measuring resources.

In this paper, we propose an angular CA controller by first identifying the kinematic relation that governs the collision threat system, from which we derive the system state. The approach of building a kinematic-based model is a simpler and modified version of the work of Chakravarty

[8] by treating the controlled vehicle's body and the intruder's body as spheres to represent their respective size. Having the collision threat system state defined, we formulate a CA control law that will produce the required evasive motion. Using collision threat system state definition, we also construct a threat energy formulae by which the controller performance can be evaluated.

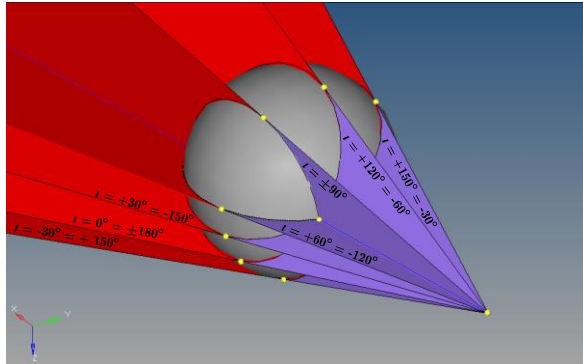


Figure 1. Evasion planes: 8 planes are described out of many (infinity) existing evasion planes

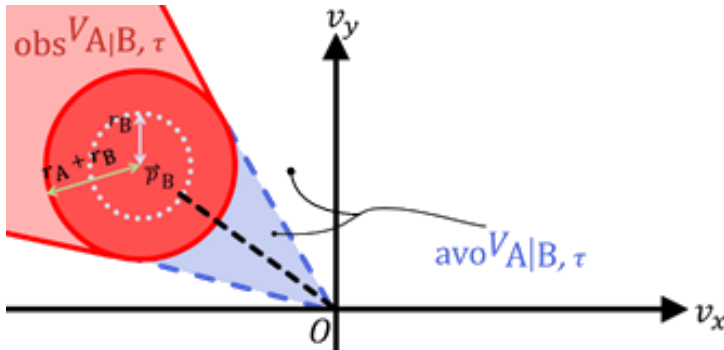


Figure 2. Geometric representation of velocity obstacle to body A in the presence of body B, in velocity space [9]

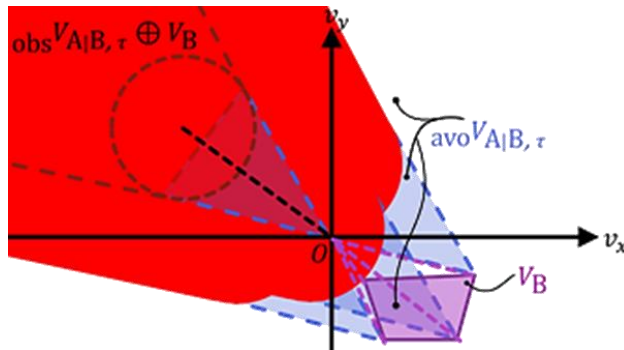


Figure 3. Velocity obstacle to body A in the presence of body B, considering all possible velocity of body B [9]

2. The Collision Threat System & Collision Avoidance

A. Collision threat detection

A.1. Collision threat situation (CTS) model: The static observer's perspective approach

We consider a UAV with a finite-size body. Regardless to its shape, a virtual sphere is defined around the UAV such that its body is fully enveloped by the sphere. The virtual sphere serves as

a forbidden space where any foreign object cannot wander into. Now we consider a typical encounter situation, where two bodies, UAV A at point A and UAV B at point B, are in motion within the vicinity of each other. A typical collision threat situation (CTS) occurs when given a certain initial condition, the projected position of both UAVs some time in the future coincide with each other occupying the same space, *e.g.*, in the vicinity of point C (Figure 4 and Figure 5). Motion variables and parameters associated with this situation are listed in Table 1. For a collision between UAV A and UAV B to occur, it is necessary that both bodies are relatively approaching each other, and that the line-of-sight angle α (or β) does not change during the remaining time before both bodies arrive at the estimated collision at point C (Figure 4). These conditions can be expressed as

$$\frac{d\|\vec{r}_{AB}\|}{dt} < 0 \tag{1}$$

$$\dot{\alpha} = 0 \quad \text{for} \quad r_A = r_B = 0 \tag{2}$$

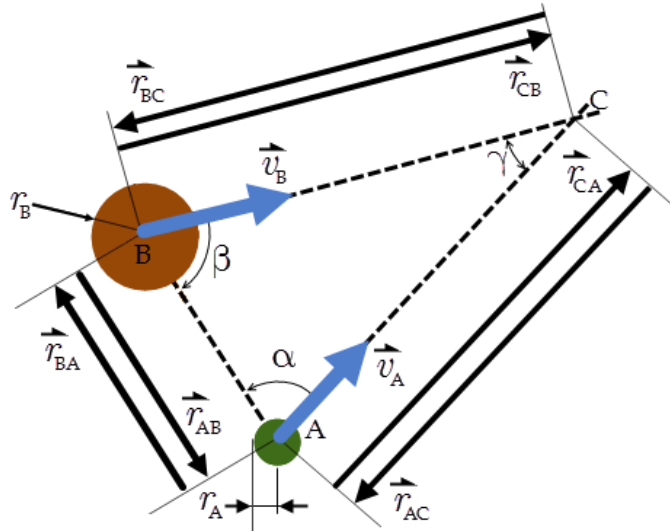


Figure 4. Collision threat situation: Collision point is estimated using point mass consideration.

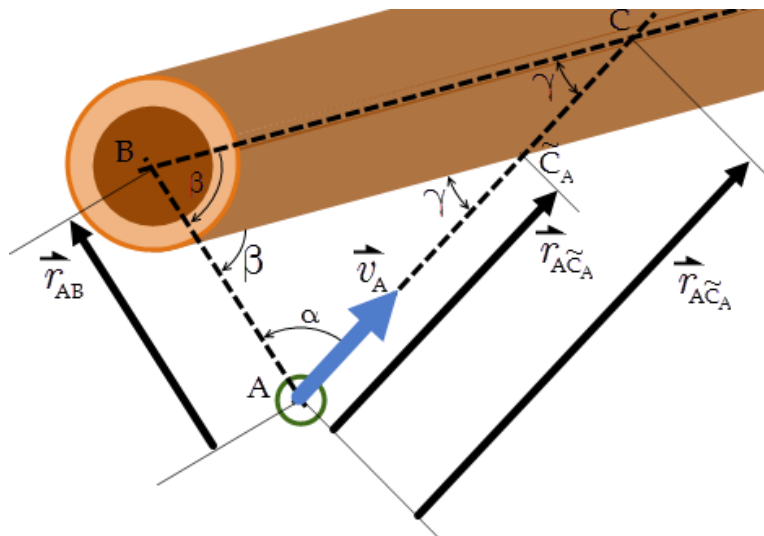


Figure 5. Collision threat situation: Collision point is estimated using finite-size body consideration.

Table 1. Parameters and Variables described in Figure 4 & Figure 5

	Variable/parameter	Symbol	Relation with other parameters
Inertial motion variables	Vector of position of UAV A & of UAV B	\vec{r}_A, \vec{r}_B	relative to a static observer
	Vector of position of estimated collision point C	\vec{r}_C	relative to a static observer
	Vector of velocity of UAV A & of UAV B	\vec{v}_A, \vec{v}_B	relative to a static observer
Relative motion variables	Vector of position of UAV A relative to UAV B	\vec{r}_{AB}	$\vec{r}_A - \vec{r}_B$ (3)
	Vector of position of UAV B relative to UAV A	\vec{r}_{BA}	$\vec{r}_B - \vec{r}_A$ (4)
	Vector of position of UAV A relative to the estimated collision point (point C)	\vec{r}_{AC}	$\vec{r}_A - \vec{r}_C$ (5)
	Vector of position of UAV B relative to the estimated collision point (point C)	\vec{r}_{BC}	$\vec{r}_B - \vec{r}_C$ (6)
	Vector of velocity of UAV A relative to UAV B	\vec{v}_{AB}	$\vec{v}_A - \vec{v}_B$ (7)
	Vector of velocity of UAV B relative to UAV A	\vec{v}_{BA}	$\vec{v}_B - \vec{v}_A$ (8)
	Line-of-sight angle: The angle constructed by the line-of-sight of relative position of UAV B to UAV A and the line-of-sight of relative position of estimated collision point C to UAV A	α	$\cos \alpha = \vec{r}_{CA}^T \cdot \vec{r}_{BA}$ $\ \sin \alpha\ = \ \vec{r}_{CA} \times \vec{r}_{BA}\ $ (9)
	Line-of-sight angle: The angle constructed by the line-of-sight of relative position of UAV A to UAV B and the line-of-sight of relative position of estimated collision point C to UAV B	β	$\cos \beta = \vec{r}_{CB}^T \cdot \vec{r}_{AB}$ $\ \sin \beta\ = \ \vec{r}_{CB} \times \vec{r}_{AB}\ $ (10)
	Estimated collision angle between UAV A and UAV B	γ	$\alpha + \beta + \gamma = \pi$ (11)
	Encounter angle: The angle constructed by the vector of relative position and the vector of relative velocity	ψ_{enc} , or $(\psi_{AB}$ or $\psi_{BA})$	(see Figure 6 & Figure 7)
	Miss angle: The angle constructed by the vector of relative position and a line tangent to the forbidden sphere's surface	ψ_{miss}	(see Figure 8)
	To-evade angle: The angle constructed by the vector of relative velocity to line tangent to the forbidden sphere's surface	ψ_{eva}	(see Figure 8)
Intrinsic parameter	Radius of forbidden sphere around UAV A	r_A	independent parameter
	Radius of forbidden sphere around UAV B	r_B	independent parameter

Condition expressed by equation (2) is valid only if both bodies is infinitesimally small in size that they both can be represented as point masses. For bodies with finite size, it is necessary that the change of the line-of-sight angle between both bodies does not exceed certain value during the remaining time before the estimated collision. These condition can be expressed as (12). The finiteness of body size is taken into account by describing the projected path of one body, *e.g.*, UAV B's body, as a thick trail instead of a thin trail. The thickness of the trail corresponds to the cumulative size of both UAV A's and UAV B's bodies. Meanwhile, the path of the other body (UAV A's) is described as a thin line. The estimated collision point now is \tilde{C}_A instead of C (Figure 5) where both UAV A and UAV B are in contact on each other's forbidden sphere surface.

$$\int_{t_A}^{t_{C_A}} \dot{\alpha} \cdot dt \leq \Delta\alpha_{miss}, \quad \Delta\alpha_{miss} > 0, \quad r_A, r_B > 0 \quad (12)$$

To evaluate the first necessary condition expressed in (1), we need to determine the remaining time before the estimated collision occurs, or the estimated time-to-collide (ETC).

$$\text{ETC}_{AB(t)} = \frac{\|\vec{r}_{AB}\|_{(t)} - (r_A + r_B + r_{\text{clear}})}{-\|\vec{v}_{r,AB(t)}\|} \quad (13)$$

$\vec{v}_{r,AB}$ is the radial part of vector \vec{v}_{AB} , which is its projection on the direction of vector \vec{r}_{AB} . If \vec{r}_{AB} and \vec{v}_{AB} are known, $\vec{v}_{r,AB}$ can be calculated using (15)-(17). The tangential part is calculated using (18)-(21) for later use.

$$\vec{v}_{AB(t)} = \vec{v}_{r,AB(t)} + \vec{v}_{l,AB(t)} \quad (14)$$

$$\vec{v}_{r,AB(t)} = v_{r,AB(t)} \cdot \vec{i}_{\vec{r}_{AB(t)}} \quad (15)$$

$$v_{r,AB} = \frac{d\|\vec{r}_{AB}\|}{dt} = \|\vec{v}_{AB}\| \cdot \cos \psi_{AB} = \frac{\vec{r}_{AB}^T \cdot \vec{v}_{AB}}{\|\vec{r}_{AB}\|} \quad (16)$$

$$\vec{i}_{\vec{r}_{AB(t)}} = \frac{\vec{r}_{AB(t)}}{\|\vec{r}_{AB}\|_{(t)}} \quad (17)$$

$$\vec{v}_{l,AB(t)} = v_{l,AB(t)} \cdot \vec{i}_{\vec{v}_{l,AB(t)}} \quad (18)$$

$$v_{l,AB} = \|\vec{v}_{AB}\| \cdot \sin \psi_{AB} = \frac{\|\vec{r}_{AB} \times \vec{v}_{AB}\|}{\|\vec{r}_{AB}\|} \quad (19)$$

$$\vec{i}_{\vec{v}_{l,AB(t)}} = \vec{i}_{\vec{v}_{AB}} \times \vec{i}_{\vec{v}_{r,AB}} \quad (20)$$

$$\vec{i}_{\vec{v}_{AB}} = \frac{\vec{r}_{AB} \times \vec{v}_{AB}}{\|\vec{r}_{AB} \times \vec{v}_{AB}\|} \times \vec{i}_{\vec{r}_{AB}} \quad (21)$$

The collision event described in Figure 5 may be estimated, and a CA control law can then be formulated and a solution for any given initial condition can be calculated as long as all motion variables of both UAV A and UAV B are known. But this approach has a shortcoming. Using the CTS model described in Figure 4 and in Figure 5 means the involvement of nonpartisan resource in providing navigational data to each UAVs. As explained in section 1.B, it defeats the independency of a UAV system in executing collision avoidance autonomously. To avoid such dependency, we use another approach in modeling the CTS; we consider one of a pair of equivalent descriptions describing the same CTS in relative perspectives (Figure 6 & Figure 7) instead of that in nonpartisan perspective described in Figure 4 & Figure 5.

A.2. Collision threat situation (CTS) model: The relative perspective approach

In Figure 6, motion of UAV A and UAV B are described according to an observer on UAV B. UAV B now is treated as a static object. The forbidden spheres around both UAVs are now replaced by another forbidden sphere around UAV B whose radius now equals $r_A + r_B$; UAV A now is represented by a point object without forbidden sphere. Motion variables of UAV A now expressed in relative terms to that of UAV B. One can immediately see the direction of UAV A's relative velocity to UAV B, from which a collision may be projected to occur (or not) by inspecting whether the direction line intrudes UAV B's forbidden sphere or not. The direction line of relative velocity and the direction line of relative position (the line-of-sight) of UAV A to UAV B forms an angle at which UAV A is encountering UAV B. We name this angle as "angle of encounter" (ψ_{AB}). In Figure 7, the opposite situation takes place.

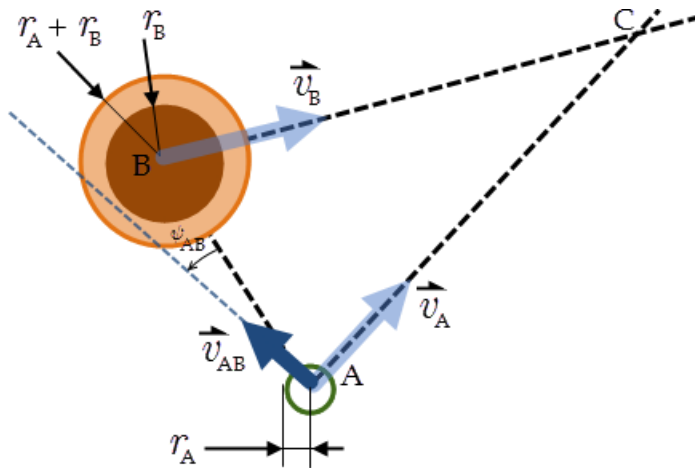


Figure 6. Collision threat situation with relative perspective of an observer on UAV B.

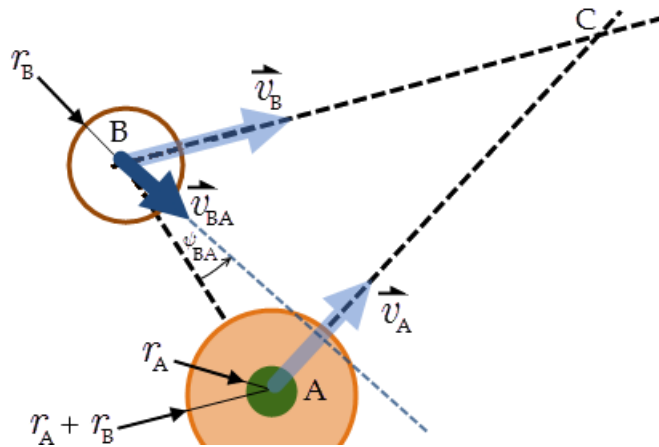


Figure 7. Collision threat situation with relative perspective of an observer on UAV A.

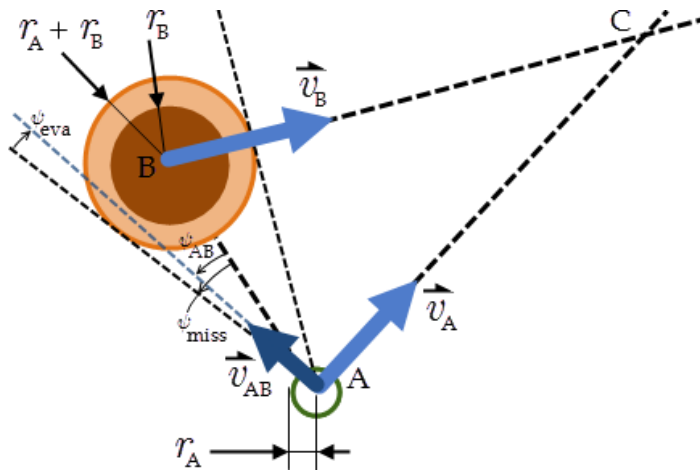


Figure 8. Angle of encounter ψ_{AB} , miss angle ψ_{miss} , and to-evade angle ψ_{eva}

From this point forward, we will be using the first description (Figure 6) of the relative perspective approach to describe the CTS unless it is stated otherwise. Beside all variables and parameters described in Table 1 and the newly-introduced encounter angle ψ_{AB} , we will also be

considering miss angle $\psi_{AB\text{miss}}$ (or ψ_{miss}), and to-evade angle $\psi_{AB\text{eva}}$ (or ψ_{eva}). The miss angle ψ_{miss} is an angle encounter with the least possible value that leads to a miss condition. The to-evade angle ψ_{eva} is the difference between the miss angle ψ_{miss} and ψ_{AB} , or $\psi_{\text{eva}} = \psi_{\text{miss}} - \psi_{AB}$. The geometric definition of these two angles is described in Figure 8.

To evaluate the second necessary condition (12) for encounter case involving finite-size bodies, we consider the angle of encounter ψ_{AB} and the miss angle $\psi_{AB\text{miss}}$ (Figure 8). For UAV A to collide with UAV B, the magnitude of angle of encounter must be consistently less than the magnitude of miss angle (22) during the remaining time before the estimated collision.

$$\|\psi_{AB}\| < \|\psi_{AB\text{miss}}\|, \quad t_0 \leq t < t_0 + ETC \quad (22)$$

Therefore, we can express the second necessary condition in (12) as (23).

$$\int_0^{ETC} \dot{\psi}_{AB} \cdot dt \leq \psi_{\text{eva}}, \quad \psi_{\text{eva}} = \psi_{\text{miss}} - \psi_{AB}, \quad r_A, r_B > 0 \quad (23)$$

B. One-on-one collision avoidance kinematics

The kinematic constraint between UAV A and UAV B during an encounter event is described geometrically in Figure 9. We consider the tangential distance y between vector \vec{v}_{AB} to point B (UAV B's center point).

$$y = \|\vec{r}_{AB}\| \cdot \sin\|\psi_{AB}\| \quad (24)$$

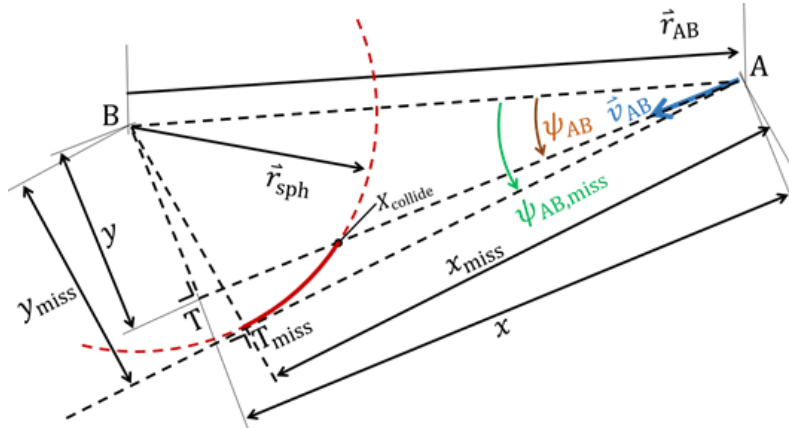


Figure 9. Relation between change in angle of encounter and tangential distance y

$y_{\vec{v}_{AB}} = y$ is the projected value of the radial distance of A relative to B when the magnitude of encounter angle $\|\psi_{AB}\|$ equals $\frac{\pi}{2}$ radian. If y is less than $\|\vec{r}_{AB}\|$ when $\|\psi_{AB}\|$ equals $\frac{\pi}{2}$ radian, UAV A will move along trajectory \widehat{AT} , and collision is estimated to occur at a point along curve $\widehat{X_{\text{collide}}T_{\text{miss}}}$ (Figure 9). To avoid collision, the value of y must be sufficiently large so that UAV A will move along trajectory $\widehat{AT}_{\text{miss}}$ instead. This is achieved by making the rate of change of $\|\psi_{AB}\|$ exceeds the critical value. This critical value can be calculated by evaluating the time differential of $\|\psi_{AB}\|$ in (24).

$$\dot{y} = \frac{d\|\vec{r}_{AB}\|}{dt} \cdot \sin\|\psi_{AB}\| + \frac{d\|\psi_{AB}\|}{dt} \cdot \|\vec{r}_{AB}\| \cdot \cos\|\psi_{AB}\| \quad (25)$$

Under CTS, equation (25) is constrained by (1). Therefore, any performing collision avoidance controller must provide that the rate of change of tangential distance y is sufficiently high to cover the required distance to evade collision within the remaining time-to-collide (26).

$$\frac{d\|\vec{r}_{AB}\|}{dt} < 0 \quad (1)$$

$$\dot{y} > \frac{y_{\text{miss}} - y}{ETC_{AB}} = \frac{\|\vec{r}_{AB}\| \cdot (\sin\|\psi_{\text{miss}}\| - \sin\|\psi_{AB}\|)}{ETC_{AB}} \quad (26)$$

Substituting these two constraints into equation (25), we have

$$\frac{d\|\psi_{AB}\|}{dt} > \frac{(\sin\|\psi_{\text{miss}}\| - \sin\|\psi_{AB}\|)}{ETC_{AB} \cdot \cos\|\psi_{AB}\|} \quad (27)$$

Substituting (13) into (27), we have

$$\frac{d\|\psi_{AB}\|}{dt} > \frac{-\|\vec{v}_{r,AB}\|}{(\|\vec{r}_{AB}\| - r_{\text{fsph}})} \cdot \frac{(\sin\|\psi_{\text{miss}}\| - \sin\|\psi_{AB}\|)}{\cos\|\psi_{AB}\|} \quad (28)$$

with $r_{\text{sph}} = r_A + r_B + r_{\text{clear}}$. r_{clear} is the prescribed clearance distance between UAVs. We define the right-hand side of inequality (28) as the state of the collision threat system.

$$\xi_{\text{CTS}} := \frac{-\|\vec{v}_{r,AB}\|}{(\|\vec{r}_{AB}\| - r_{\text{fsph}})} \cdot \frac{(\sin\|\psi_{\text{miss}}\| - \sin\|\psi_{AB}\|)}{\cos\|\psi_{AB}\|} \quad (29)$$

Inequality (28) is a set of solution that satisfies (23). By equaling both sides of inequality (28), we get an expression that describes the critical condition between miss and hit (collision). Inequality (28) also provides us an insight about the state variable of a collision threat system: It depends on the vector of relative position \vec{r}_{AB} and the vector of relative velocity \vec{v}_{AB} . Furthermore, both vectors lie on a plane in three-dimensional space that intersect the forbidden sphere at its center point (Figure 10). A computer-aided design (CAD) tool can be used to prove geometrically that this plane offers the shortest path for vector \vec{v}_{AB} to reach $\vec{v}_{AB\text{miss}}$ (Figure 11). We then exploit this fact to formulate a collision avoiding control action.

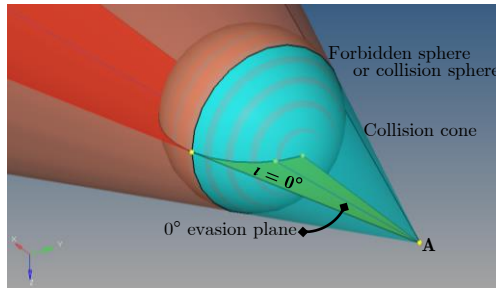


Figure 10. The zero-inclination evasion plane

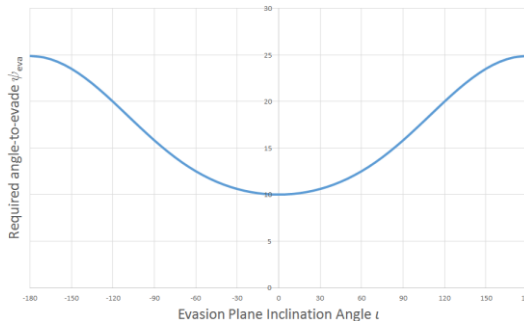


Figure 11. Variation of to-evade angle to evasion plane inclination

The cross product of the vector of encounter angle rate of change $\bar{\omega}_{AB}$ with the vector of relative velocity \bar{v}_{AB} gives the required translational relative acceleration of UAV A to avoid collision with UAV B.

$$\dot{\bar{v}}_{CA} = \bar{\omega}_{CA} \times \bar{v}_{AB} \quad (30)$$

$$\bar{\omega}_{CA} = \left. \frac{d \|\psi_{AB}\|}{dt} \right|_{CA} \cdot \bar{i}_{\psi_{AB}} \quad (31)$$

$$u_{CA} = \left. \frac{d \|\psi_{AB}\|}{dt} \right|_{CA} := k_{CA} \cdot \xi_{CTS} \quad (32)$$

k_{CA} is the CA controlling gain k_{CA} . To satisfy inequality (28), k_{CA} must be greater than 1 ($k_{CA} > 1$).

The processes described by (13)-(32) is summarized in a control diagram Figure 12.

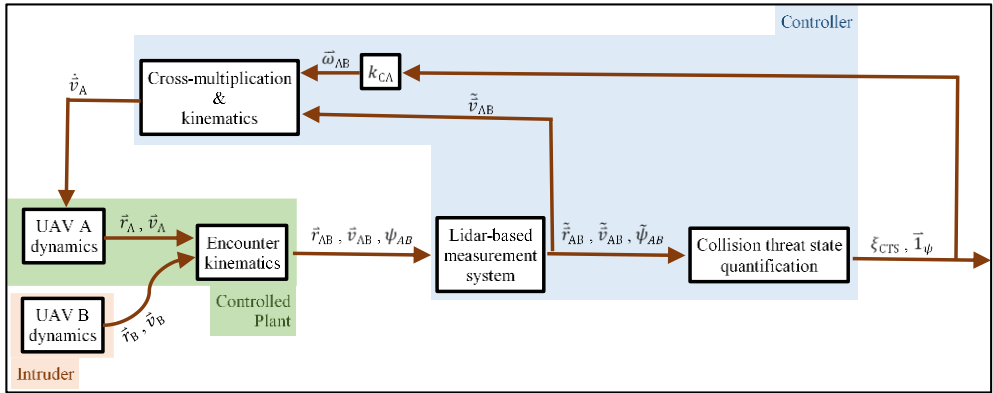


Figure 12. Collision avoidance control system diagram

Recalling (7), evasive action (30) can be expressed in term of non-relative variables. Hence,

$$\dot{\bar{v}}_A - \dot{\bar{v}}_B = \bar{\omega}_{AB,eva} \times (\bar{v}_A - \bar{v}_B) \quad (33)$$

or

$$\dot{\bar{v}}_A = \bar{\omega}_{AB,eva} \times \bar{v}_A =: u_{CA,A} \quad (34)$$

$$\dot{\bar{v}}_B = \bar{\omega}_{AB,eva} \times \bar{v}_B =: u_{CA,B} \quad (35)$$

Equations (34) and (35) are the required CA controller's action on each party. These equations also describe an interesting fact of collision avoiding nature between a pair of vehicles. The evasive action can be contributed by either party, resulting a non-cooperative CA action. But if both parties contribute, the CA control system shows cooperative behavior, and the cost of CA action is shared. This behavior is shown and discussed in subsection 3.B.3.

C. Collision Avoidance Control System Stability Analysis

We evaluate the stability of the collision avoidance control system by examining the energy E of the threat system when CA controller (32) is applied to the collision threat system. This approach follows Lyapunov's formalized idea that a system must be stable if its total energy is dissipated. The collision threat system's energy consists of potential energy and kinetic energy, each of which has a radial part and an angular part, as described by (36)-(38). Their respective rate of change is described by (39)-(41).

$$E = EP + EK \quad (36)$$

$$EP = EP_{\text{rad}} + EP_{\text{ang}} \quad (37)$$

$$EK = EK_{\text{rad}} + EK_{\text{ang}} \quad (38)$$

$$\frac{dE}{dt} = \frac{dEP}{dt} + \frac{dEK}{dt} \quad (39)$$

$$\frac{dEP}{dt} = \frac{dEP_{\text{rad}}}{dt} + \frac{dEP_{\text{ang}}}{dt} \quad (40)$$

$$\frac{dEK}{dt} = \frac{dEK_{\text{rad}}}{dt} + \frac{dEK_{\text{ang}}}{dt} \quad (41)$$

Before proceeding further, we define two variables, q and p , that will be the state variables in the energy equations.

$$q_{\text{rad}} := \frac{1}{\|\vec{r}_{\text{AB}}\|} - \frac{1}{\infty} = \frac{1}{\|\vec{r}_{\text{AB}}\|} \quad (42)$$

$$q_{\text{ang}} := \frac{1}{\|\psi_{\text{enc}}\|} - \frac{1}{\|\psi_{\text{miss}}\|} \quad (43)$$

$$p_{\text{rad}} := \dot{q}_{\text{rad}} \quad (44)$$

$$p_{\text{ang}} := \dot{q}_{\text{ang}} \quad (45)$$

with $\psi_{\text{enc}} = \psi_{\text{AB}}$. We also have the time-derivatives for (42) (43), (44), & (45).

$$\dot{q}_{\text{rad}} = -\frac{\frac{d}{dt}\|\vec{r}_{\text{AB}}\|}{\|\vec{r}_{\text{AB}}\|^2} \quad (46)$$

$$\ddot{q}_{\text{rad}} = -\frac{1}{\|\vec{r}_{\text{AB}}\|^2} \cdot \left(\frac{d^2\|\vec{r}_{\text{AB}}\|}{dt^2} - \frac{2}{\|\vec{r}_{\text{AB}}\|} \cdot \left(\frac{d\|\vec{r}_{\text{AB}}\|}{dt} \right)^2 \right) \quad (47)$$

$$\dot{q}_{\text{ang}} := \frac{1}{\|\psi_{\text{miss}}\|^2} \cdot \frac{d\|\psi_{\text{miss}}\|}{dt} - \frac{1}{\|\psi_{\text{enc}}\|^2} \cdot \frac{d\|\psi_{\text{enc}}\|}{dt} \quad (48)$$

Since $\frac{d\|\psi_{\text{miss}}\|}{d\|\psi_{\text{enc}}\|} = 0$, and by chain rule $\frac{d\|\psi_{\text{miss}}\|}{dt} = \frac{d\|\psi_{\text{miss}}\|}{d\|\psi_{\text{enc}}\|} \cdot \frac{d\|\psi_{\text{enc}}\|}{dt}$, then $\frac{d\|\psi_{\text{miss}}\|}{dt} = 0$ in (48).

$$\dot{q}_{\text{ang}} := -\frac{1}{\|\psi_{\text{enc}}\|^2} \cdot \frac{d\|\psi_{\text{enc}}\|}{dt} \quad (49)$$

$$\ddot{q}_{\text{ang}} := -\frac{1}{\|\psi_{\text{enc}}\|^2} \cdot \left(\frac{d^2\|\psi_{\text{enc}}\|}{dt^2} - \frac{2}{\|\psi_{\text{enc}}\|} \cdot \left(\frac{d\|\psi_{\text{enc}}\|}{dt} \right)^2 \right) \quad (50)$$

$$\dot{p}_{\text{rad}} = \ddot{q}_{\text{rad}} \quad (51)$$

$$\dot{p}_{\text{ang}} = \ddot{q}_{\text{ang}} \quad (52)$$

C.1. Collision threat system's potential energy

The radial potential energy is a function of inversed radial distance between the evading UAV (UAV A) and the collision threat source (UAV B). Likewise, the angular potential energy is a function of inversed angular distance, that is, the magnitude of the angle of encounter ψ_{enc} between the evading UAV and the collision threat source.

$$EP_{\text{rad}} = k_{EP_{\text{rad}}} \cdot q_{\text{rad}} = \frac{k_{EP_{\text{rad}}}}{\|\vec{r}_{AB}\|} \quad (53)$$

$$EP_{\text{ang}} = k_{EP_{\text{ang}}} \cdot q_{\text{ang}} = k_{EP_{\text{ang}}} \cdot \left(\frac{1}{\|\psi_{\text{enc}}\|} - \frac{1}{\|\psi_{\text{miss}}\|} \right) \quad (54)$$

$k_{EP_{\text{rad}}}$ and $k_{EP_{\text{ang}}}$ are coefficients that represent the product of inertia property of the evading UAV with a weighing parameter.

The time-derivative of threat system's potential energy can then be derived.

$$\frac{dEP_{\text{rad}}}{dt} = k_{EP_{\text{rad}}} \cdot \dot{q}_{\text{rad}} = -\frac{k_{EP_{\text{rad}}}}{\|\vec{r}_{AB}\|^2} \cdot \frac{d\|\vec{r}_{AB}\|}{dt} \quad (55)$$

$$\frac{dEP_{\text{ang}}}{dt} = k_{EP_{\text{ang}}} \cdot \dot{q}_{\text{ang}} = -\frac{k_{EP_{\text{ang}}}}{\|\psi_{\text{enc}}\|^2} \cdot \frac{d\|\psi_{\text{enc}}\|}{dt} \quad (56)$$

Evaluating (55) and (56) for condition when (1) and (32) is applied in collision threat situation,

$$\frac{d\|\vec{r}_{AB}\|}{dt} < 0 \quad (1)$$

$$\frac{dEP_{\text{rad}}}{dt} > 0 \quad (57)$$

$$\left. \frac{d\|\psi_{\text{enc}}\|}{dt} \right|_{\text{CA}} := k_{\text{CA}} \cdot \xi_{\text{CTS}} = k_{\text{CA}} \cdot \frac{1}{ETC} \cdot \frac{(\sin\|\psi_{\text{miss}}\| - \sin\|\psi_{\text{enc}}\|)}{\cos\|\psi_{\text{enc}}\|} \quad (32)$$

$$\frac{dEP_{\text{ang}}}{dt} = -k_{\text{CA}} \cdot k_{EP_{\text{ang}}} \cdot \frac{(\sin\|\psi_{\text{miss}}\| - \sin\|\psi_{\text{enc}}\|)}{ETC \cdot \|\psi_{\text{enc}}\|^2 \cdot \cos\|\psi_{\text{enc}}\|}$$

$$\frac{dEP_{\text{ang}}}{dt} \leq 0, \quad \forall k_{\text{CA}} \geq 0 \quad (58)$$

The radial part of potential energy rate (57) is always increasing under CTS regardless the application of CA controller (32). On the other hand, the angular part (58) is negative as long as CA controller gain k_{CA} is positive. Equating the sum of these two parts to a non-positive value, we get

$$\left. \begin{aligned} \frac{dEP}{dt} &\leq 0 \\ \frac{dEP_{\text{rad}}}{dt} + \frac{dEP_{\text{ang}}}{dt} &\leq 0 \end{aligned} \right\} \quad (59)$$

$$k_{\text{CA}} \geq -\frac{k_{EP_{\text{rad}}}}{k_{EP_{\text{ang}}}} \cdot \frac{d\|\bar{r}_{\text{AB}}\|}{dt} \cdot \frac{ETC \cdot \|\psi_{\text{enc}}\|^2 \cdot \cos\|\psi_{\text{enc}}\|}{\|\bar{r}_{\text{AB}}\|^2 \cdot (\sin\|\psi_{\text{miss}}\| - \sin\|\psi_{\text{enc}}\|)} \quad (60)$$

C.2. Collision threat system's kinetic energy

Threat kinetic energy also consists of radial and angular components. The radial kinetic energy (61) is a function of the rate of change of radial distance. And the angular kinetic energy (62) is a function of the rate of change of angular distance.

$$\begin{aligned} EK_{\text{rad}} &= \frac{1}{2} k_{EK_{\text{rad}}} \cdot p_{\text{rad}}^2 \\ &= \frac{1}{2} \frac{k_{EK_{\text{rad}}}}{\|\bar{r}_{\text{AB}}\|^4} \cdot \left(\frac{d\|\bar{r}_{\text{AB}}\|}{dt} \right)^2 \end{aligned} \quad (61)$$

$$\begin{aligned} EK_{\text{ang}} &= \frac{1}{2} k_{EK_{\text{ang}}} \cdot p_{\text{ang}}^2 \\ &= \frac{1}{2} \frac{k_{EK_{\text{ang}}}}{\|\psi_{\text{enc}}\|^4} \cdot \left(\frac{d\|\psi_{\text{enc}}\|}{dt} \right)^2 \end{aligned} \quad (62)$$

Like in (53) and (54), $k_{EK_{\text{rad}}}$ and $k_{EK_{\text{ang}}}$ in (61) and (62) are coefficients representing the product of inertia property of the evading UAV with a weighing parameter.

The time-derivative of threat system's kinetic energy can then be derived.

$$\begin{aligned} \frac{dEK_{\text{rad}}}{dt} &= k_{EK_{\text{rad}}} \cdot p_{\text{rad}} \cdot \dot{p}_{\text{rad}} \\ &= \frac{k_{EK_{\text{rad}}}}{\|\bar{r}_{\text{AB}}\|^4} \cdot \frac{d\|\bar{r}_{\text{AB}}\|}{dt} \cdot \left(\frac{d^2\|\bar{r}_{\text{AB}}\|}{dt^2} - \frac{2}{\|\bar{r}_{\text{AB}}\|} \cdot \left(\frac{d\|\bar{r}_{\text{AB}}\|}{dt} \right)^2 \right) \end{aligned} \quad (63)$$

$$\begin{aligned} \frac{dEK_{\text{ang}}}{dt} &= k_{EK_{\text{ang}}} \cdot p_{\text{ang}} \cdot \dot{p}_{\text{ang}} \\ &= \frac{k_{EK_{\text{ang}}}}{\|\psi_{\text{enc}}\|^4} \cdot \frac{d\|\psi_{\text{enc}}\|}{dt} \cdot \left(\frac{d^2\|\psi_{\text{enc}}\|}{dt^2} - \frac{2}{\|\psi_{\text{enc}}\|} \cdot \left(\frac{d\|\psi_{\text{enc}}\|}{dt} \right)^2 \right) \end{aligned} \quad (64)$$

Evaluating (63) and (64) for condition when (1) and (32) are applied in collision threat situation, we have

$$\frac{d\|\bar{r}_{\text{AB}}\|}{dt} < 0 \quad (1)$$

$$\frac{dEK_{\text{rad}}}{dt} \leq 0 \quad \text{if} \quad \frac{d^2\|\bar{r}_{\text{AB}}\|}{dt^2} \geq -\frac{2}{\|\bar{r}_{\text{AB}}\|} \cdot \left(\frac{d\|\bar{r}_{\text{AB}}\|}{dt} \right)^2 \quad (65)$$

$$\left. \frac{d\|\psi_{\text{enc}}\|}{dt} \right|_{\text{CA}} := k_{\text{CA}} \cdot \xi_{\text{CTS}} = k_{\text{CA}} \cdot \frac{1}{ETC} \cdot \frac{(\sin\|\psi_{\text{miss}}\| - \sin\|\psi_{\text{enc}}\|)}{\cos\|\psi_{\text{enc}}\|} \quad (32)$$

$$\frac{dEK_{\text{ang}}}{dt} \leq 0 \quad \text{if} \quad \frac{d^2\|\psi_{\text{enc}}\|}{dt^2} \leq \frac{2}{\|\psi_{\text{enc}}\|} \cdot \left(\frac{k_{\text{CA}}}{ETC} \cdot \frac{(\sin\|\psi_{\text{miss}}\| - \sin\|\psi_{\text{enc}}\|)}{\cos\|\psi_{\text{enc}}\|} \right)^2 \quad (66)$$

Inequality (65) shows that a sufficiently high deceleration in radial direction to the threat source is required for the radial kinetic energy to decrease. So far, the CA controller (32) works in angular direction. If we wish to extend our CA controller design to operate in the radial direction, inequality (65) provides us a firm starting point to do it.

Meanwhile, inequality (66) describes that angular kinetic energy rate of change is proportional to angular acceleration. Equation for angular acceleration can be obtained by deriving the time-derivative of (32).

$$\begin{aligned} \left. \frac{d^2\|\psi_{\text{enc}}\|}{dt^2} \right|_{\text{CA}} &= \frac{dk_{\text{CA}}}{dt} \cdot \xi_{\text{CTS}} + k_{\text{CA}} \cdot \frac{d\xi_{\text{CTS}}}{dt} \leq 0 \\ \frac{dk_{\text{CA}}}{dt} \cdot \xi_{\text{CTS}} + k_{\text{CA}} \cdot \frac{d\xi_{\text{CTS}}}{dt} &\leq 0 \\ \frac{dk_{\text{CA}}}{dt} &\leq -\frac{k_{\text{CA}}}{\xi_{\text{CTS}}} \cdot \frac{d\xi_{\text{CTS}}}{dt} \end{aligned} \quad (67)$$

Then, we use (67) to substitute the conditional part of (66).

$$\frac{dEK_{\text{ang}}}{dt} \leq 0 \quad \text{if} \quad \frac{dk_{\text{CA}}}{dt} \leq -\frac{k_{\text{CA}}}{\xi_{\text{CTS}}} \cdot \frac{d\xi_{\text{CTS}}}{dt} \quad (68)$$

C.3. Summary on threat system's energy evaluation

For the threat system to be stable in the sense of Lyapunov, the summation of all energy rate equations (55), (56), (63), and (64) must be less than or equal zero when the CA control action (32) is applied in the collision threat situation (1).

$$\left. \begin{aligned} \frac{dE}{dt} &\leq 0 \\ \frac{dEP_{\text{rad}}}{dt} + \frac{dEP_{\text{ang}}}{dt} + \frac{dEK_{\text{rad}}}{dt} + \frac{dEK_{\text{ang}}}{dt} &\leq 0 \end{aligned} \right\} \quad (69)$$

With $\frac{dEP_{\text{rad}}}{dt} > 0$, we must ensure that the other three terms in (69) are negative enough that (69) is satisfied, or

$$\left. \frac{dEP_{\text{ang}}}{dt} + \frac{dEK_{\text{rad}}}{dt} + \frac{dEK_{\text{ang}}}{dt} \leq -\frac{dEP_{\text{rad}}}{dt} \right\} \quad (70)$$

We can do this by ensuring these following conditions are satisfied.

$$k_{\text{CA}} \geq 0 \quad (58)$$

$$\frac{d^2\|\vec{r}_{\text{AB}}\|}{dt^2} \geq -\frac{2}{\|\vec{r}_{\text{AB}}\|} \cdot \left(\frac{d\|\vec{r}_{\text{AB}}\|}{dt} \right)^2 \quad (65)$$

$$\frac{dk_{\text{CA}}}{dt} \leq -\frac{k_{\text{CA}}}{\xi_{\text{CTS}}} \cdot \frac{d\xi_{\text{CTS}}}{dt} \quad (67)$$

3. Simulation

A. Simulation setup

We conduct some simulations to assess our CA controller performance to the variation of the applied controller gain k_{CA} . According to (58), any positive value is sufficient. For this, we consider a CTS with side encounter in three cases, namely Case #1, #2, and #3, representing the use of gain values 1, 10, and 50 applied by CA controller on UAV A (UAV #01). Except the CA controller gain value, these three cases are identical. UAV B (UAV #02) is the non-cooperative intruder whose CA controller gain values is set to zero. Summaries of the setup are presented in Table 2 - Table 4.

To emphasize the controller capability in three-dimensional motion, we also simulate side encounter cases, with UAV having different initial positions (Case #4, #5, and #6). Summaries are presented in Table 5 - Table 7.

Lastly, a couple simulations are set up to observe the capability of our CA controller to perform a cooperative CA. The first case (Case #7) represents a non-cooperative CA case where CA controller gain k_{CA} of UAV A is set to one and k_{CA} of UAV B is set to zero. In the other case (Case #8), CA controller gain k_{CA} of both UAVs are set to one, thus representing a cooperative CA case. The case setup is summarized in Table 8 (Case #7) and Table 9 (Case #8).

Table 2. Case #1: Side encounter, CA gain on UAV A = 1

UAV A		
Parameter name	Value	Unit
Size (by spherical radius), r_A	10	Unit length, absolute.
Initial position, $\vec{r}_{A(t_0)}$	$[0 \ -46 \ 0]^T$	Unit distance, w.r.t. inertial coordinate system
Initial velocity, $\vec{v}_{A(t_0)}$	$[0 \ 6 \ 0]^T$	Unit velocity, w.r.t. inertial coordinate system
CA controller gain, $k_{AB,eva}$	1	
UAV B		
Parameter name	Value	Unit
Size (by spherical radius), r_B	10	Unit length, absolute
Initial position, $\vec{r}_{B(t_0)}$	$[-46 \ 0 \ 0]^T$	Unit distance, w.r.t. inertial coordinate system
Initial velocity, $\vec{v}_{B(t_0)}$	$[6 \ 0 \ 0]^T$	Unit velocity, w.r.t. inertial coordinate system
CA controller gain, $k_{BA,eva}$	0	
Encounter parameter		
Prescribed clearance distance between UAVs, r_{clear}	5	Unit distance, absolute.
Prescribed evasion zone:	$r_A + r_B + r_{clear}$	Unit distance, absolute.

Table 3. Case #2: Side encounter, CA gain on UAV A = 10

UAV A		
Parameter name	Value	Unit
Size (by spherical radius), r_A	10	Unit length, absolute.
Initial position, $\vec{r}_{A(t_0)}$	$[0 \ -46 \ 0]^T$	Unit distance, w.r.t. inertial coordinate system
Initial velocity, $\vec{v}_{A(t_0)}$	$[0 \ 6 \ 0]^T$	Unit velocity, w.r.t. inertial coordinate system
CA controller gain, $k_{AB,eva}$	10	
UAV B		
Parameter name	Value	Unit
Size (by spherical radius), r_B	10	Unit length, absolute
Initial position, $\vec{r}_{B(t_0)}$	$[-46 \ 0 \ 0]^T$	Unit distance, w.r.t. inertial coordinate system
Initial velocity, $\vec{v}_{B(t_0)}$	$[6 \ 0 \ 0]^T$	Unit velocity, w.r.t. inertial coordinate system
CA controller gain, $k_{BA,eva}$	0	
Encounter parameter		
Prescribed clearance distance between UAVs, r_{clear}	5	Unit distance, absolute.
Prescribed evasion zone:	$r_A + r_B + r_{clear}$	Unit distance, absolute.

Table 4. Case #3: Side encounter, CA gain on UAV A = 50

UAV A		
Parameter name	Value	Unit
Size (by spherical radius), r_A	10	Unit length, absolute.
Initial position, $\vec{r}_{A(t_0)}$	$[0 \ -46 \ 0]^T$	Unit distance, w.r.t. inertial coordinate system
Initial velocity, $\vec{v}_{A(t_0)}$	$[0 \ 6 \ 0]^T$	Unit velocity, w.r.t. inertial coordinate system
CA controller gain, $k_{AB,eva}$	50	
UAV B		
Parameter name	Value	Unit
Size (by spherical radius), r_B	10	Unit length, absolute
Initial position, $\vec{r}_{B(t_0)}$	$[-46 \ 0 \ 0]^T$	Unit distance, w.r.t. inertial coordinate system
Initial velocity, $\vec{v}_{B(t_0)}$	$[6 \ 0 \ 0]^T$	Unit velocity, w.r.t. inertial coordinate system
CA controller gain, $k_{BA,eva}$	0	
Encounter parameter		
Prescribed clearance distance between UAVs, r_{clear}	5	Unit distance, absolute.
Prescribed evasion zone:	$r_A + r_B + r_{clear}$	Unit distance, absolute.

Table 5. Case #5: Side encounter, UAV A's alt. = UAV B's alt.

UAV A		
Parameter name	Value	Unit
Size (by spherical radius), r_A	10	Unit length, absolute.
Initial position, $\vec{r}_{A(t_0)}$	$[0 \ -46 \ 0]^T$	Unit distance, w.r.t. inertial coordinate system
Initial velocity, $\vec{v}_{A(t_0)}$	$[0 \ 6 \ 0]^T$	Unit velocity, w.r.t. inertial coordinate system
CA controller gain, $k_{AB,CA}$	1	
UAV B		
Parameter name	Value	Unit
Size (by spherical radius), r_B	10	Unit length, absolute
Initial position, $\vec{r}_{B(t_0)}$	$[-46 \ 0 \ 0]^T$	Unit distance, w.r.t. inertial coordinate system
Initial velocity, $\vec{v}_{B(t_0)}$	$[6 \ 0 \ 0]^T$	Unit velocity, w.r.t. inertial coordinate system
CA controller gain, $k_{BA,CA}$	0	
Encounter parameter		
Prescribed clearance distance between UAVs, r_{clear}	5	Unit distance, absolute.
Prescribed evasion zone:	$r_A + r_B + r_{clear}$	Unit distance, absolute.

Table 6. Case #4: Side encounter, UAV A's alt. < UAV B's alt.

UAV A		
Parameter name	Value	Unit
Size (by spherical radius), r_A	10	Unit length, absolute.
Initial position, $\vec{r}_{A(t_0)}$	$[-5 \ -46 \ -5]^T$	Unit distance, w.r.t. inertial coordinate system
Initial velocity, $\vec{v}_{A(t_0)}$	$[0 \ 6 \ 0]^T$	Unit velocity, w.r.t. inertial coordinate system
CA controller gain, $k_{AB,CA}$	1	
UAV B		
Parameter name	Value	Unit
Size (by spherical radius), r_B	10	Unit length, absolute
Initial position, $\vec{r}_{B(t_0)}$	$[-46 \ 0 \ 0]^T$	Unit distance, w.r.t. inertial coordinate system
Initial velocity, $\vec{v}_{B(t_0)}$	$[6 \ 0 \ 0]^T$	Unit velocity, w.r.t. inertial coordinate system
CA controller gain, $k_{BA,CA}$	0	
Encounter parameter		
Prescribed clearance distance between UAVs, r_{clear}	5	Unit distance, absolute.
Prescribed evasion zone:	$r_A + r_B + r_{clear}$	Unit distance, absolute.

Table 7. Case #6: Side encounter, UAV A's alt. > UAV B's alt.

UAV A		
Parameter name	Value	Unit
Size (by spherical radius), r_A	10	Unit length, absolute.
Initial position, $\vec{r}_{A(t_0)}$	[5 -46 5] ^T	Unit distance, w.r.t. inertial coordinate system
Initial velocity, $\vec{v}_{A(t_0)}$	[0 6 0] ^T	Unit velocity, w.r.t. inertial coordinate system
CA controller gain, $k_{AB,CA}$	1	
UAV B		
Parameter name	Value	Unit
Size (by spherical radius), r_B	10	Unit length, absolute
Initial position, $\vec{r}_{B(t_0)}$	[-46 0 0] ^T	Unit distance, w.r.t. inertial coordinate system
Initial velocity, $\vec{v}_{B(t_0)}$	[6 0 0] ^T	Unit velocity, w.r.t. inertial coordinate system
CA controller gain, $k_{BA,CA}$	0	
Encounter parameter		
Prescribed clearance distance between UAVs, r_{clear}	5	Unit distance, absolute.
Prescribed evasion zone:	$r_A + r_B + r_{clear}$	Unit distance, absolute.

Table 8. Case #7: Front encounter (non-cooperative maneuver)

UAV A		
Parameter name	Value	Unit
Size (by spherical radius), r_A	10	Unit length, absolute.
Initial position, $\vec{r}_{A(t_0)}$	[-2.5 -46 0] ^T	Unit distance, w.r.t. inertial coordinate system
Initial velocity, $\vec{v}_{A(t_0)}$	[0 6 0] ^T	Unit velocity, w.r.t. inertial coordinate system
CA controller gain, $k_{AB,eva}$	1	
UAV B		
Parameter name	Value	Unit
Size (by spherical radius), r_B	10	Unit length, absolute
Initial position, $\vec{r}_{B(t_0)}$	[2.5 54 0] ^T	Unit distance, w.r.t. inertial coordinate system
Initial velocity, $\vec{v}_{B(t_0)}$	[0 -6 0] ^T	Unit velocity, w.r.t. inertial coordinate system
CA controller gain, $k_{BA,eva}$	0	
Encounter parameter		
Prescribed clearance distance between UAVs, r_{clear}	5	Unit distance, absolute.
Prescribed evasion zone:	$r_A + r_B + r_{clear}$	Unit distance, absolute.

Table 9. Case #8: Front encounter (cooperative maneuver)

UAV A		
Parameter name	Value	Unit
Size (by spherical radius), r_A	10	Unit length, absolute.
Initial position, $\vec{r}_{A(t_0)}$	$[-2.5 \ -46 \ 0]^T$	Unit distance, w.r.t. inertial coordinate system
Initial velocity, $\vec{v}_{A(t_0)}$	$[0 \ 6 \ 0]^T$	Unit velocity, w.r.t. inertial coordinate system
CA controller gain, $k_{AB,eva}$	1	
UAV B		
Parameter name	Value	Unit
Size (by spherical radius), r_B	10	Unit length, absolute
Initial position, $\vec{r}_{B(t_0)}$	$[2.5 \ 54 \ 0]^T$	Unit distance, w.r.t. inertial coordinate system
Initial velocity, $\vec{v}_{B(t_0)}$	$[0 \ -6 \ 0]^T$	Unit velocity, w.r.t. inertial coordinate system
CA controller gain, $k_{BA,eva}$	0	
Encounter parameter		
Prescribed clearance distance between UAVs, r_{clear}	5	Unit distance, absolute.
Prescribed evasion zone:	$r_A + r_B + r_{clear}$	Unit distance, absolute.

B. Simulation result

The performance of our proposed CA controller can be assessed by evaluating the following metrics: the change in kinetic energy (Figure 34) and the trajectory deflection (Figure 35). Lower values correspond to higher performance in executing evasion task.

Without losing generality while maintaining clarity, results are presented in two-dimensional space, *e.g.*, Figure 35 - Figure 37, since one may find it harder to make any distinction about what-is-going-where in 3D. However, results in three-dimensional space are also presented as complementary presentation, *e.g.*, Figure 38 - Figure 40. Figure 13 - Figure 22 are composite plots comprising 13 subplots each with the following arrangement from top to bottom and from left to right:

- 1) Position in global coordinate system. The circles drawn in solid line is the forbidden sphere of respective UAV, representing their physical bodies. The circles drawn in dashed line represents the forbidden sphere that includes the prescribed clearance distance r_{clear} . A collision situation, or ‘hit’, occurs if both solid-line circles comes in contact with each other. Otherwise, a ‘miss’ situation occurs, *i.e.*, collision is avoided.
- 2) Position in local coordinate system (strapped down to UAV B, or UAV #02). The circle drawn in solid line represents the forbidden sphere around UAV B without the prescribed clearance distance. A hit situation occurs if area enclosed by the circle is intruded. Forbidden sphere that includes the prescribed clearance distance r_{clear} is drawn in dashed line. A violation of safety measurement occurs if area enclosed by this circle is intruded.
- 3) Velocity in local coordinate system (strapped down to UAV B, or UAV #02).
- 4) Radial distance. The solid red horizontal line in the plot represents the radial distance that corresponds to the forbidden sphere radius described in subplot 2). A ‘hit’ situation occurs when radial distance falls below the red horizontal line.
- 5) Magnitude of relative velocity.
- 6) Relative radial velocity.

- 7) Relative tangential velocity.
- 8) Magnitude of relative acceleration.
- 9) Estimated time-to-collide (ETC). Negative gradient means both UAVs are approaching each other; positive gradient means both UAVs are moving away from each other. A ‘hit’ situation occurs when ETC value reaches the zero-line.
- 10) Encounter angle ψ_{AB} : a planar angle formed by \vec{r}_{AB} and \vec{v}_{AB} .
- 11) Miss angle ψ_{miss} : the required encounter angle that achieves miss.
- 12) Collision threat state ξ .
- 13) CA controller output.

B.1. Effect of controller gain k_{CA} to CA performance

Case #1, #2, and #3 are set up to observe how CA performance is affected by controller gain value. Initially, UAV A and UAV B are placed in separate location with enough distance between them so that each is in the outside of the other’s evasion zone. (Evasion zone is a zone where the CA controller is effectively active in responding to detected threat, *i.e.*, evasion zone is a subset of detection zone.) Initial velocities are also set in a way so that both of them starts moving in collision course with side encounter as soon as the simulation starts. During this time, the radial distance between them decreases, and while encounter angle is small, the relative velocity consists mostly of radial part with negative value, causing the estimated time-to-collide (ETC) steadily decreases, and collision threat state rises; both UAVs are in collision threat situation (CTS). They begin to intrude each other’s evasion zone at about $t = 1.77$ (Figure 13).

From this moment (Figure 14 - Figure 22), CA controller of UAV A begins working. This can be seen with the appearance of a surge of CA controller output in subplot 13). Higher gain CA controllers work sooner and with higher surge value than the lower ones. The most immediate result is the change in the relative velocity vector (subplot 3)), with the more aggressive change corresponds to higher value in CA controller gain. A notable drop in collision threat state is shown as the result (subplot 12)), especially in cases where CA gain is high, the state value drops to a value near zero, the “no-threat” condition. This is manifested in all other parameters: significant rise in encounter angle (subplot 10)), causing rise in magnitude of tangential part of relative velocity (subplot 7)). Effect in the radial direction occurs gradually where the radial part of the relative velocity change to be more positive while still be in the negative direction (subplot 6)), which results in less steep decrement in the value of ETC (subplot 9)). Apparently, both UAVs are still approaching each other but with smaller rate, and UAV A’s trajectory begins to be deflected away from UAV B, which can be seen in position space in subplots 1) & 2), more clearly in subplot 2). It can be seen that higher gain values drive UAV A away from UAV B earlier than lower gain values do. This early evasion allows UAV A to equate its encounter angle to the miss angle while there is still some distance between both UAVs, during which the miss angle is smaller than when the distance between UAVs were smaller. As a result, the trajectory deflection is smaller for high gain CA controller. Comparison of this measure is presented in Figure 34 and Figure 35. Also, early evasion allows the controller to bring the controlled vehicle out of CTS with smaller kinetic energy (Figure 34). On the other hand, controller cost for high gain CA is higher than the low gain CA (Figure 33). The opposing nature between trajectory deflection and controller effort is consistent in controller gain variation. However, this is not the case for specific kinetic energy, where variation is not monotonic according to controller gain value. Figure 34 shows that the least trajectory deflection does not always come with the least change in kinetic energy. This indicates that both measures, the trajectory deflection and the specific kinetic energy change, have a common minimum value that is not at their respective minimum, *i.e.*, there exists an optimum point for both measures.

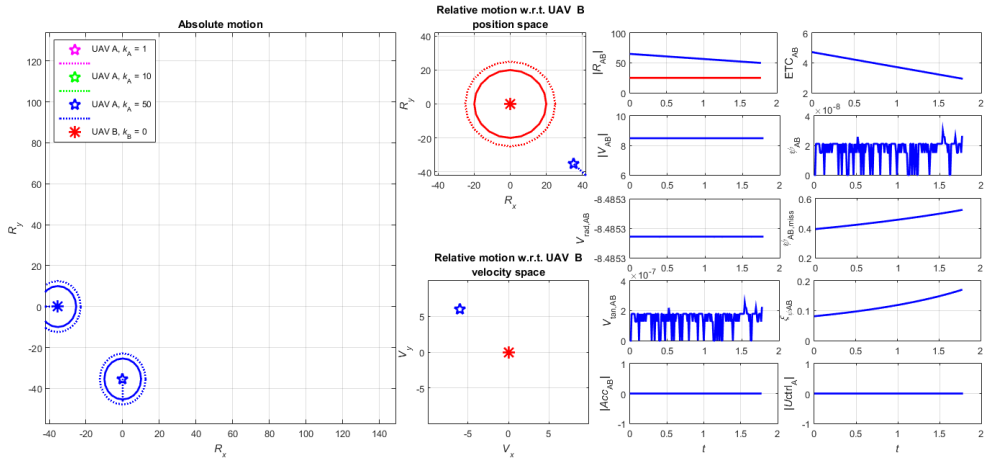


Figure 13. Case #1 (magenta), Case #2 (green), & Case #3 (blue) at $t = 1.77$.

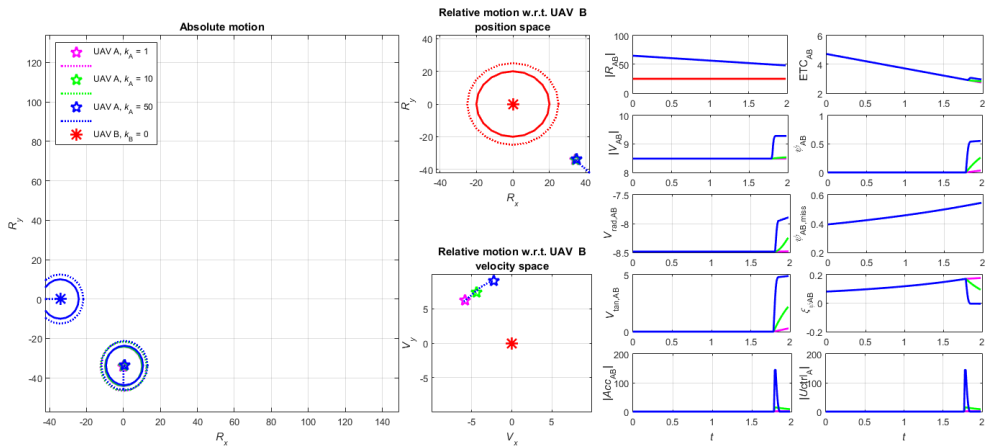


Figure 14. Case #1 (magenta), Case #2 (green), & Case #3 (blue) at $t = 1.97$.

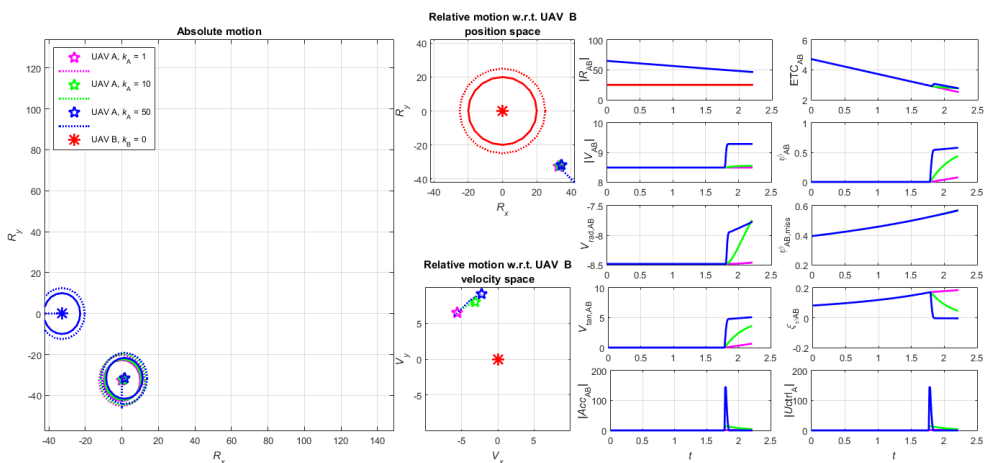


Figure 15. Case #1 (magenta), Case #2 (green), & Case #3 (blue) at $t = 2.20$.

Three-Dimensional Collision Avoidance Control for UAVs

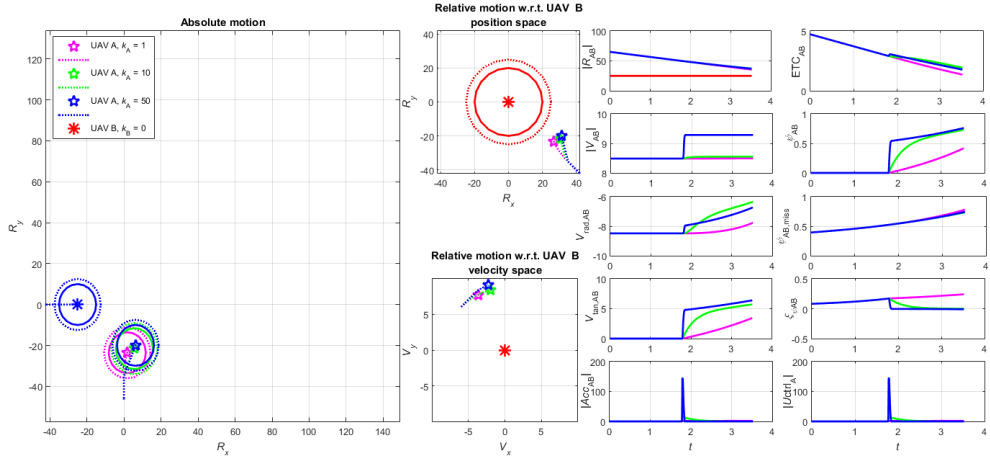


Figure 16. Case #1 (magenta), Case #2 (green), & Case #3 (blue) at $t = 3.50$.

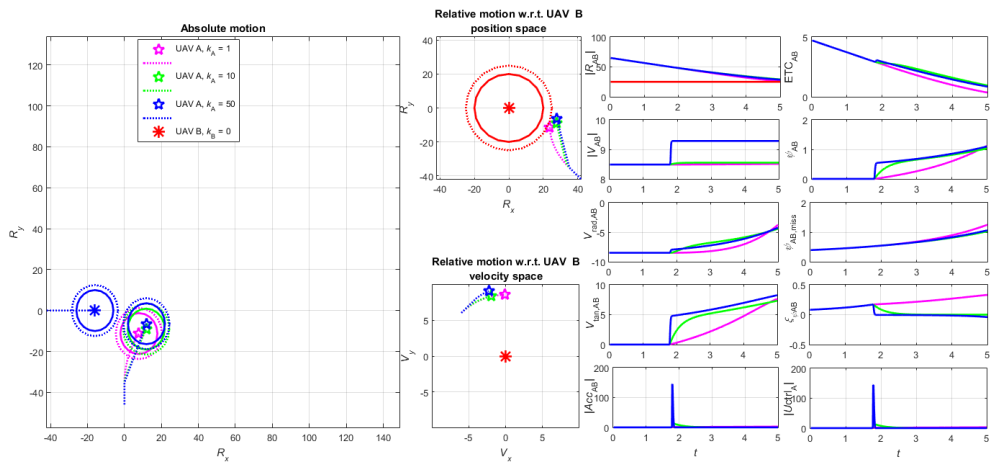


Figure 17. Case #1 (magenta), Case #2 (green), & Case #3 (blue) at $t = 5.00$.

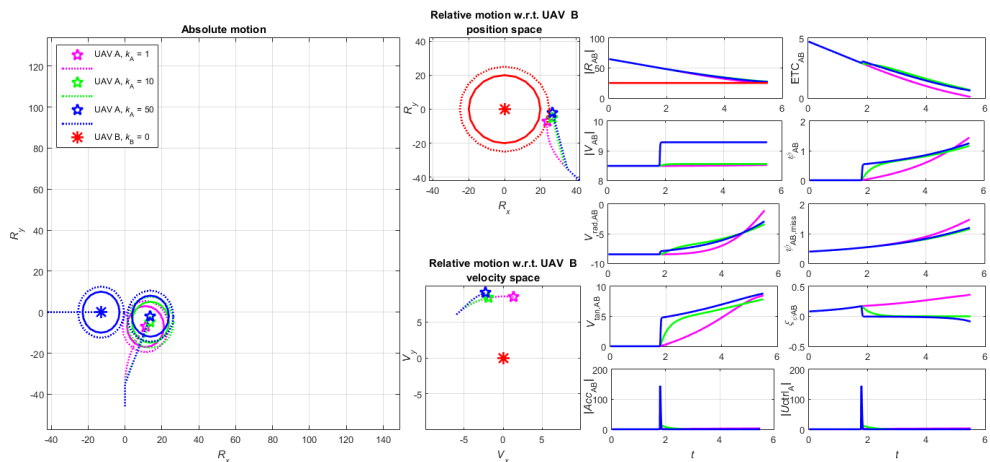


Figure 18. Case #1 (magenta), Case #2 (green), & Case #3 (blue) at $t = 5.50$.

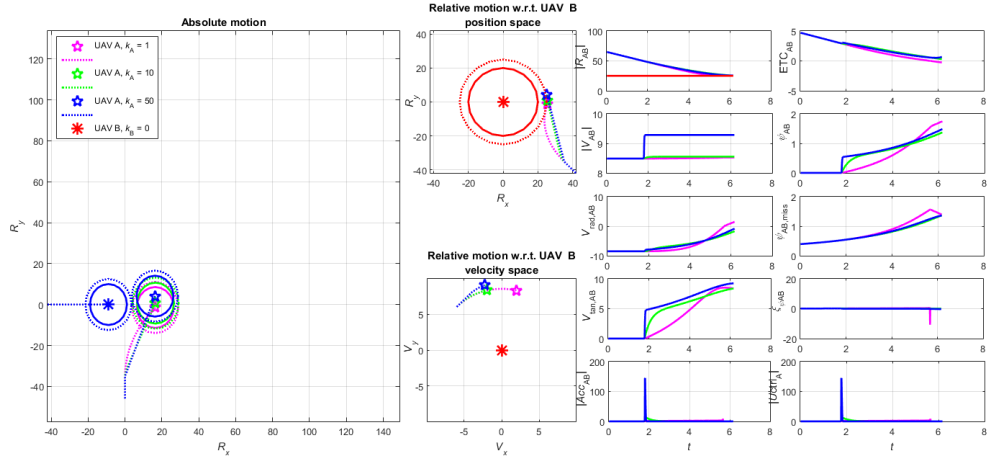


Figure 19. Case #1 (magenta), Case #2 (green), & Case #3 (blue) at $t = 6.17$.

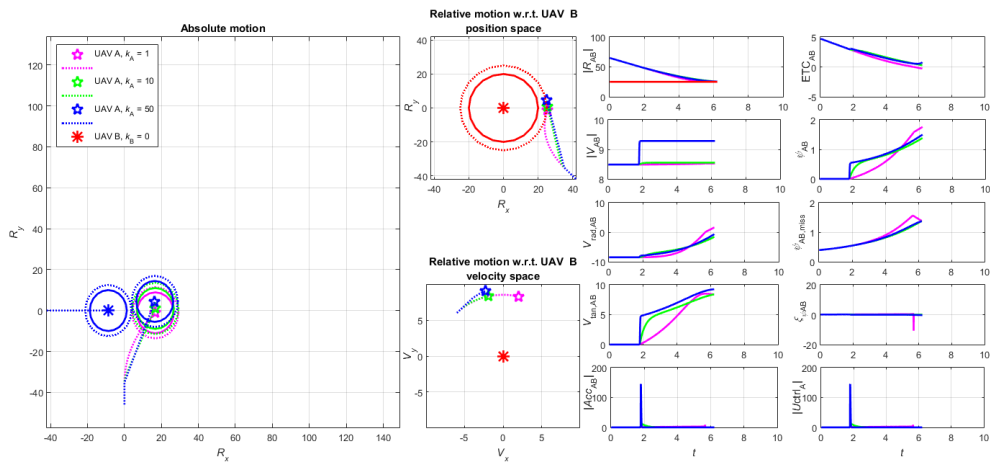


Figure 20. Case #1 (magenta), Case #2 (green), & Case #3 (blue) at $t = 6.21$.

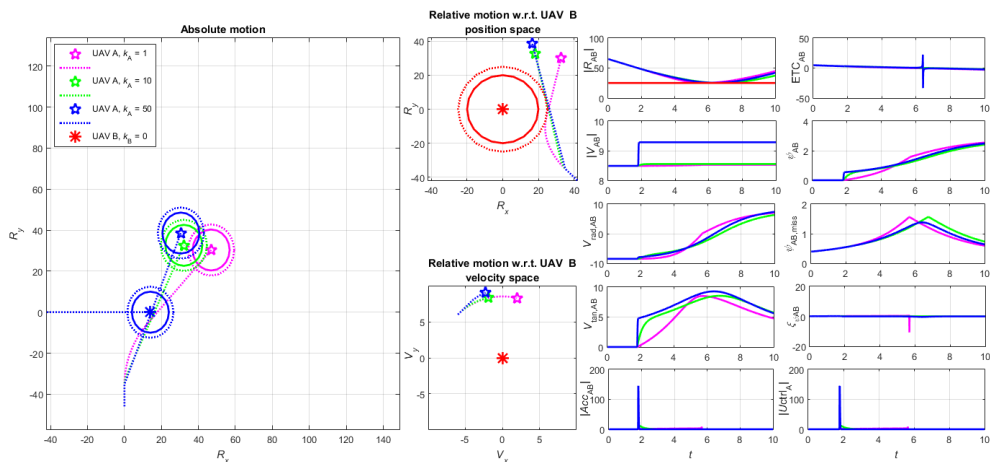


Figure 21. Case #1 (magenta), Case #2 (green), & Case #3 (blue) at $t = 10.00$.

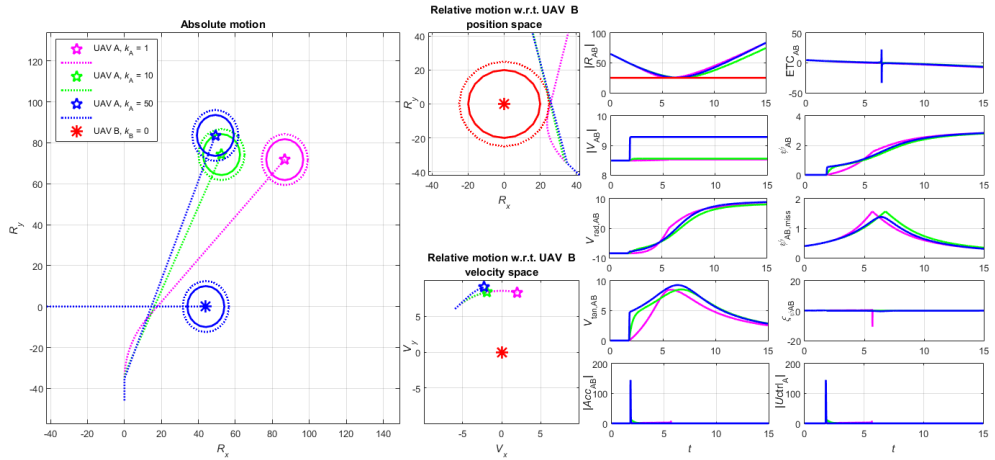


Figure 22. Case #1 (magenta), Case #2 (green), & Case #3 (blue) at $t = 15.00$.

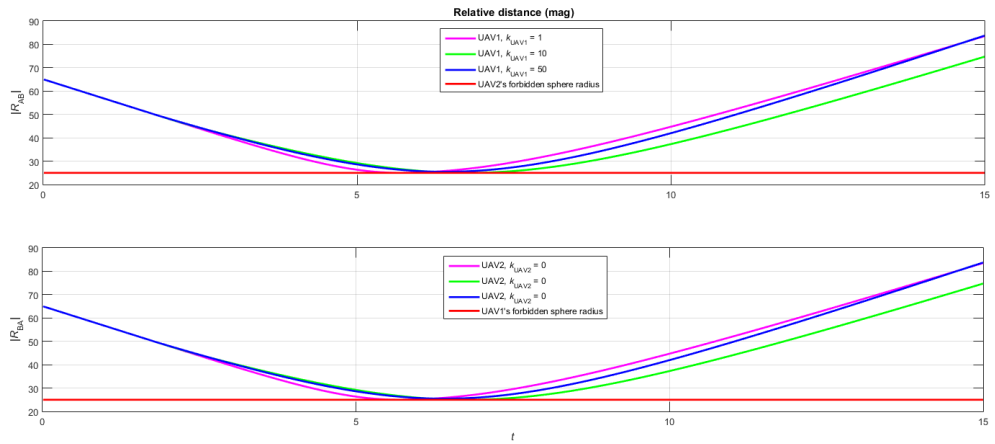


Figure 23. Relative distance of UAV A to UAV B (top), and of UAV B to UAV A (bottom)

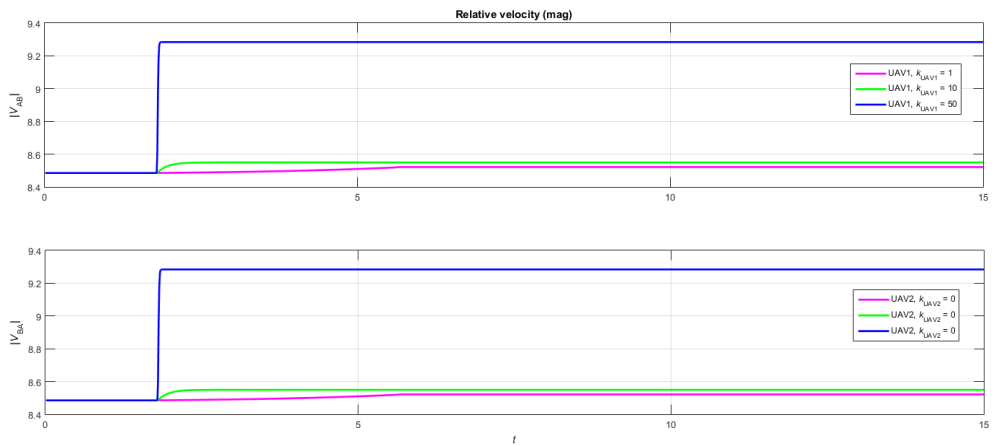


Figure 24. Relative velocity of UAV A to UAV B (top), and of UAV B to UAV A (bottom)

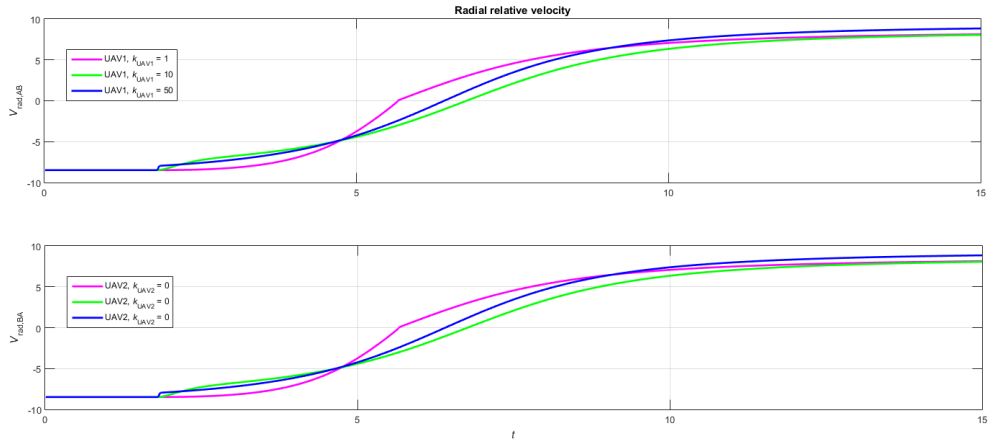


Figure 25. Relative radial velocity of UAV A to UAV B (top), and of UAV B to UAV A (bottom)

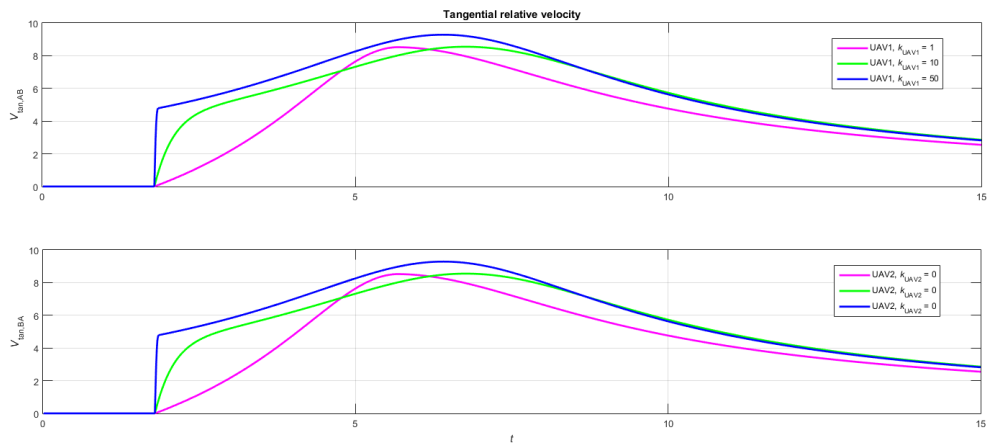


Figure 26. Relative tangential velocity of UAV A to UAV B (top), and of UAV B to UAV A (bottom)

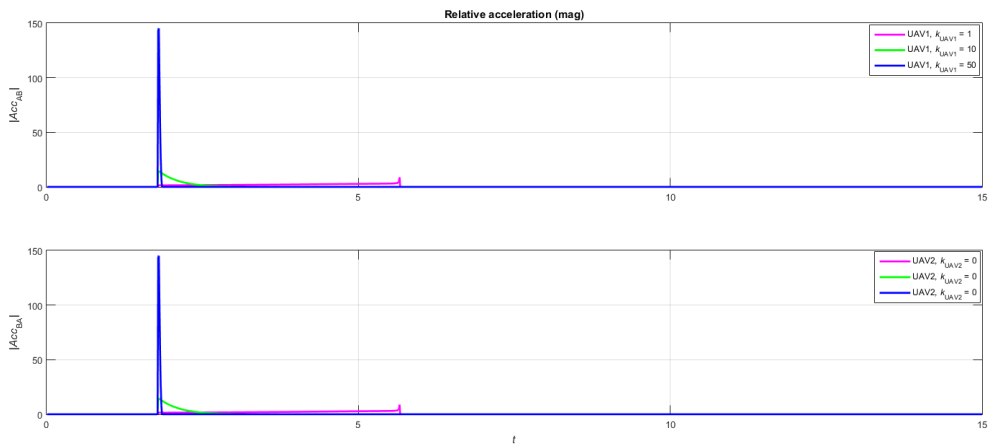


Figure 27. Relative acceleration of UAV A to UAV B (top), and of UAV B to UAV A (bottom)

Three-Dimensional Collision Avoidance Control for UAVs

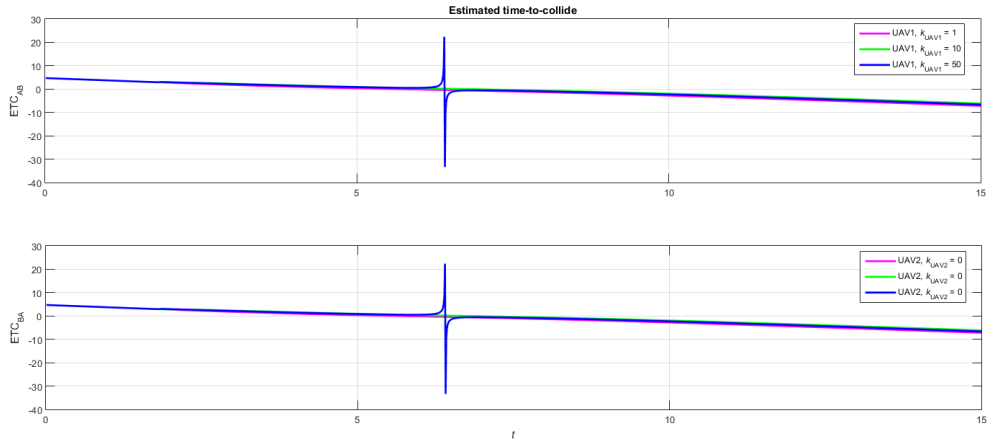


Figure 28. Estimated time-to-collide of UAV A to UAV B (top), and of UAV B to UAV A (bottom)

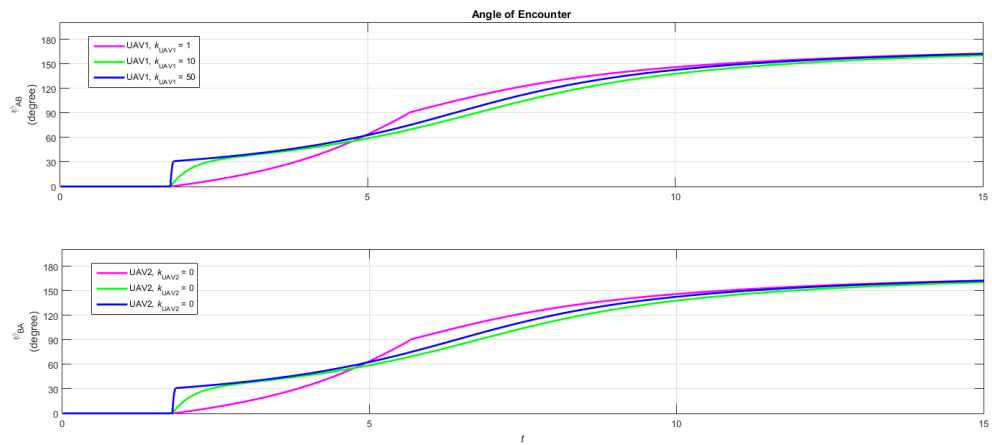


Figure 29. Encounter angle of UAV A to UAV B (top), and of UAV B to UAV A (bottom)

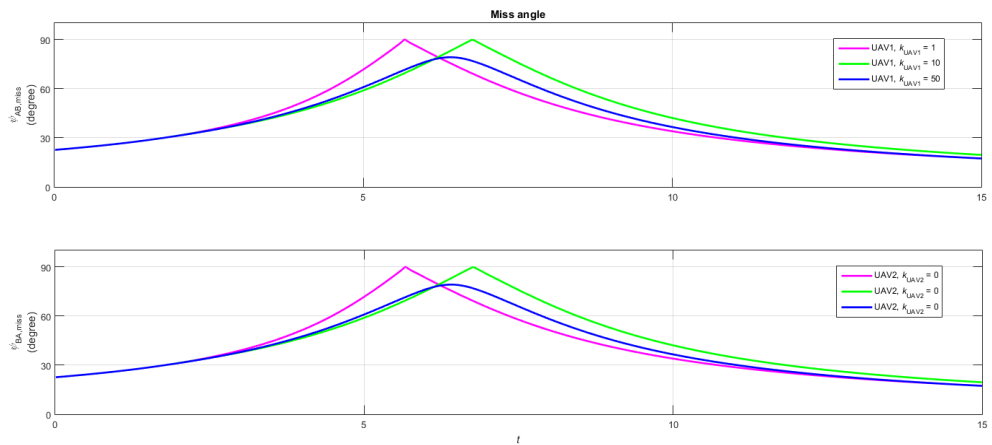


Figure 30. Miss angle of UAV A to UAV B (top), and of UAV B to UAV A (bottom)

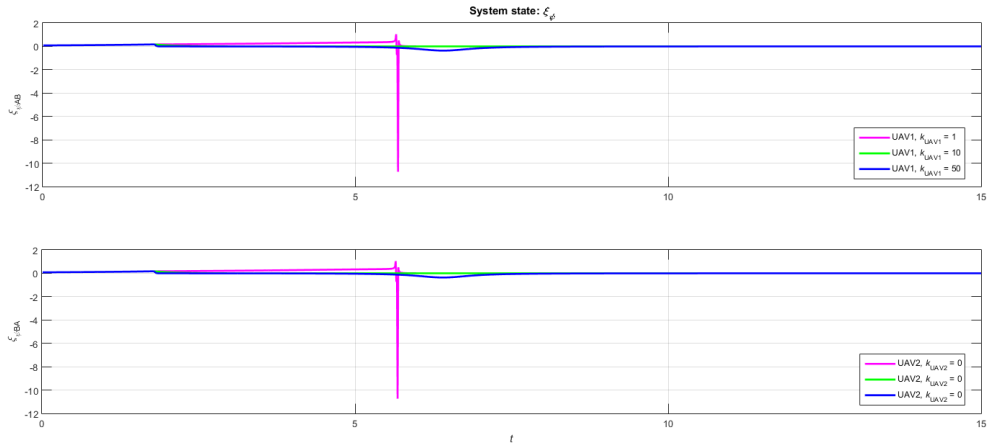


Figure 31. Collision threat system's state

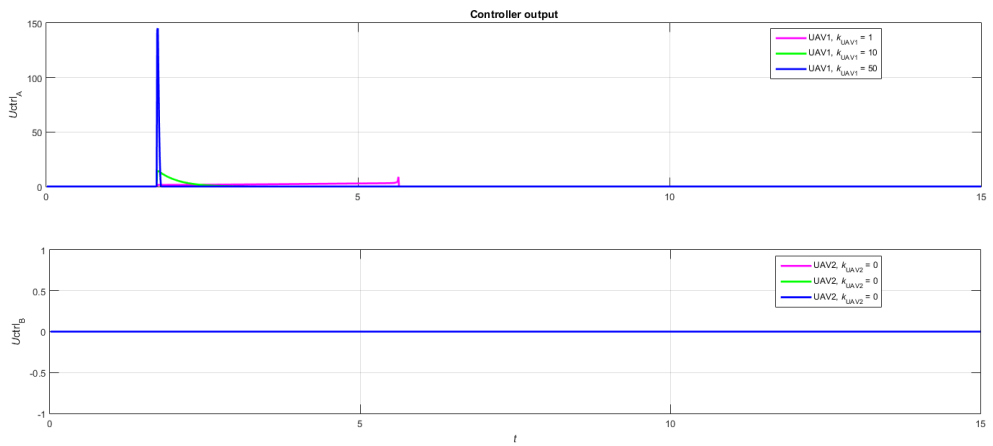


Figure 32. CA controller output on UAV A (top), and on UAV B (bottom)

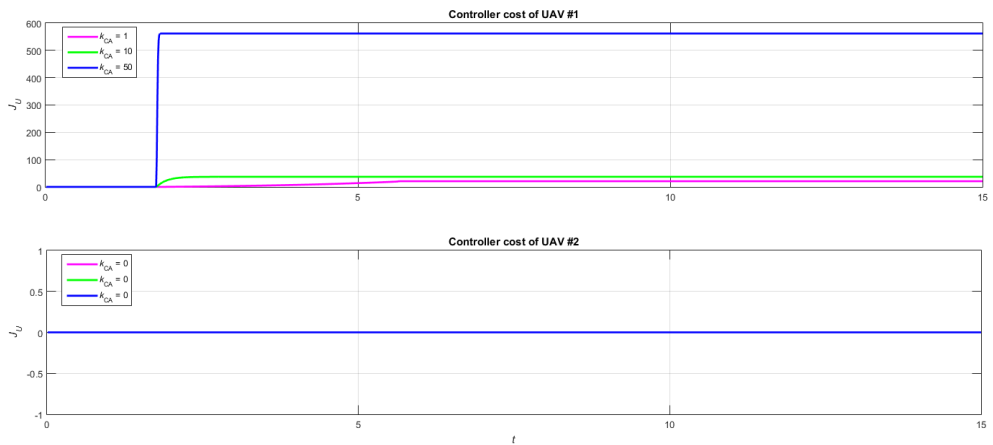


Figure 33. Controller cost of UAV A (top), and of UAV B (bottom)

Three-Dimensional Collision Avoidance Control for UAVs

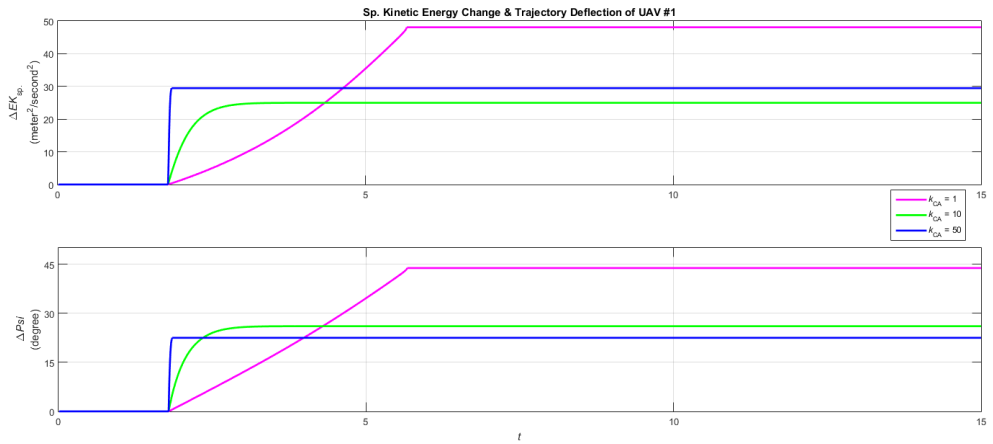


Figure 34. UAV A's evasion cost: kinetic energy change (top), and trajectory deflection (bottom)

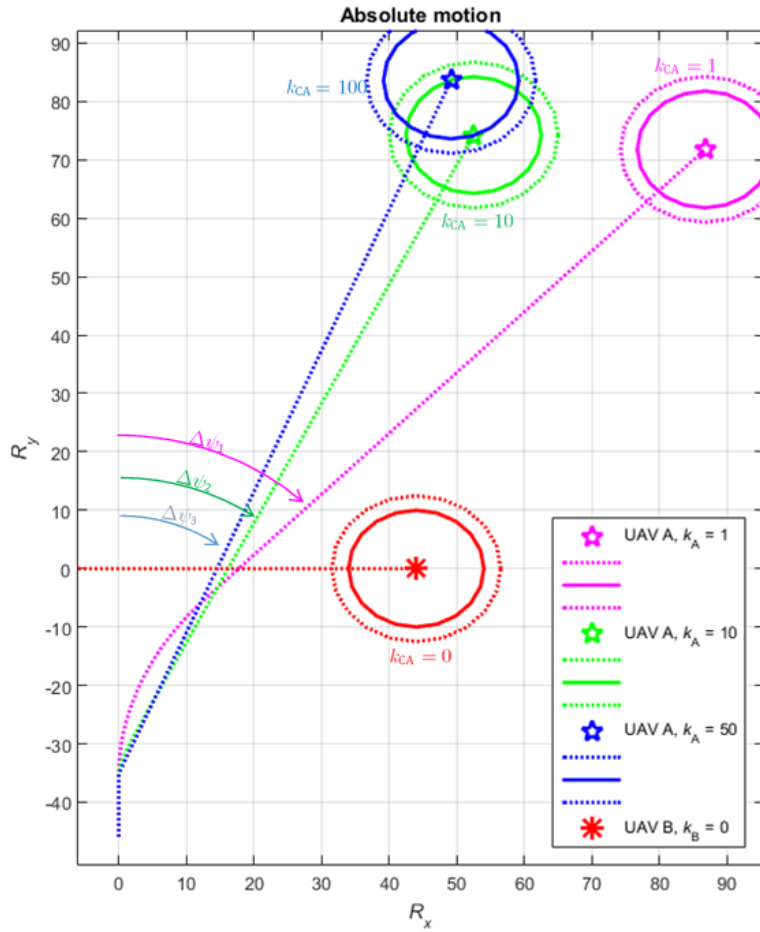


Figure 35. Trajectory deflection of UAV A as seen by a non-moving observer

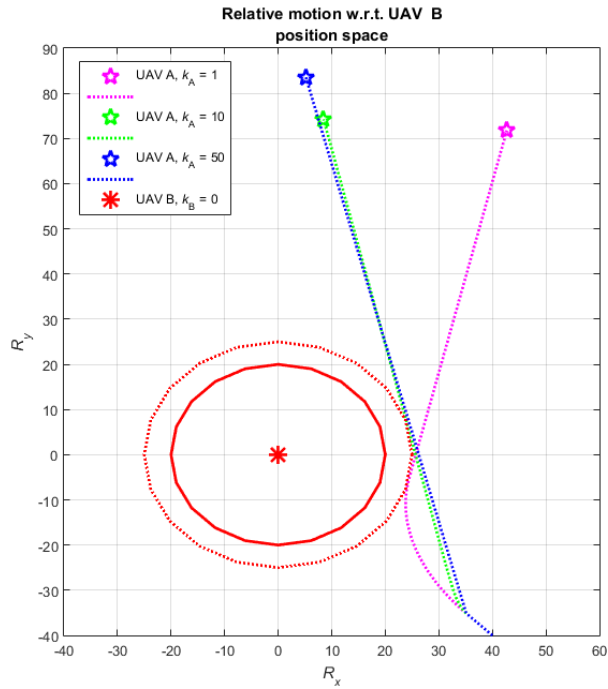


Figure 36. Trajectory deflection of UAV A as seen by UAV B

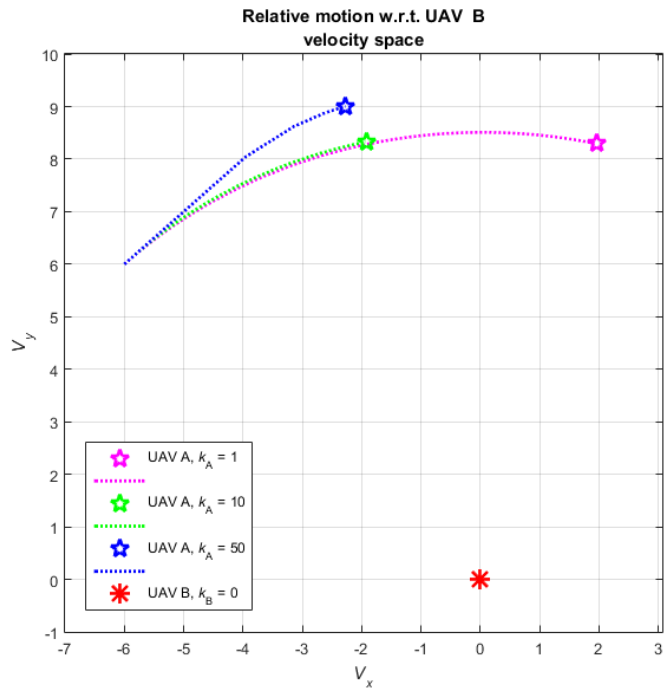


Figure 37. Velocity evolution of UAV A relative to UAV B

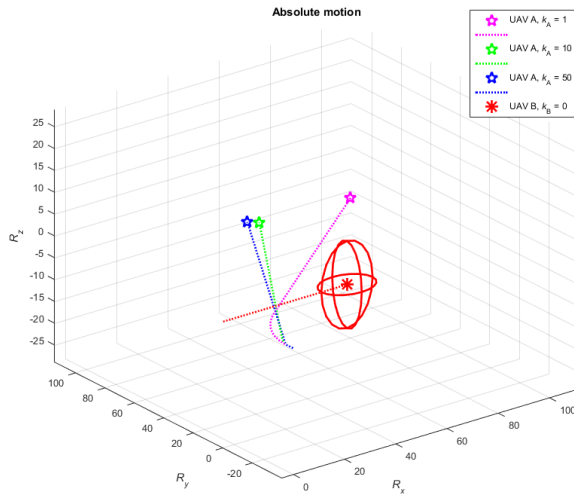


Figure 38. Position evolution of UAV A and UAV B as seen by a non-moving observer (3D)

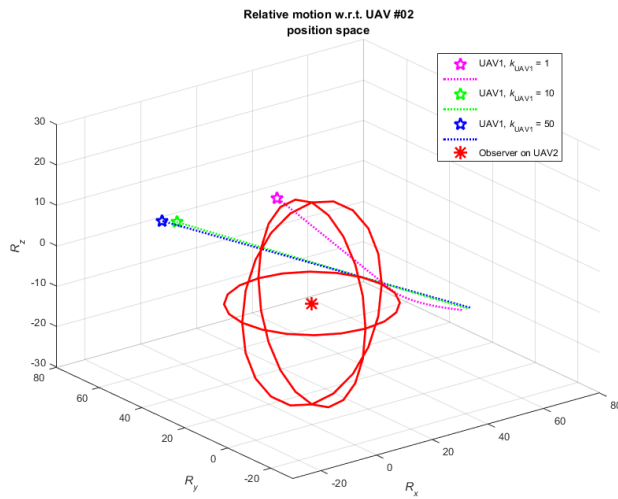


Figure 39. Position evolution of UAV A relative to UAV B as seen by UAV B (3D)

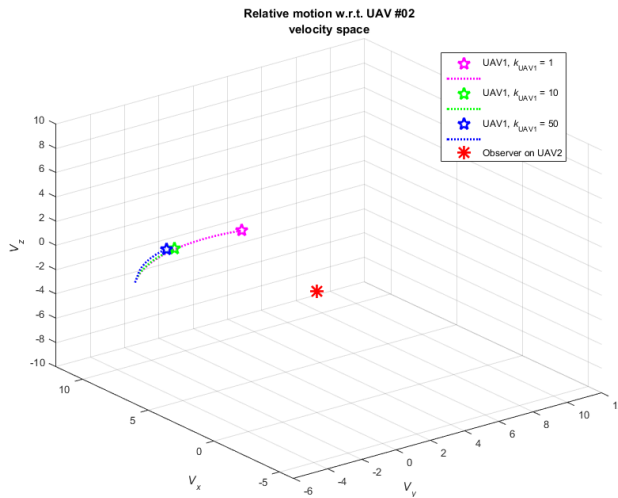


Figure 40. Velocity evolution of UAV A relative to UAV B (3D)

B.2. Three-dimensional evasion maneuver

To demonstrate and to emphasize the capability of our controller in dealing the collision threat as a three-dimensional CA problem, three similar cases as Case #1 are simulated, each with UAV A occupying different initial position such that the differences span in three-dimensional space (see Table 6 - Table 7). One case is set up with UAV A's initial position is the same as in Case #1 (Case #5). Two cases are set up with UAV A's initial position shifted both horizontally and vertically, one where the shift is leftward and downward (Case #4), and the other where the shift is rightward and upward (Case #6). If plotted on the same position space, the three initial positions form a slash character on a vertical plane whose normal direction is the direction of UAV A's initial velocity vector. With these setups, the collision threat system in each case produces different evasion maneuver. This can be seen from the resulting evasion maneuver of UAV A in each case (Figure 42 - Figure 44).

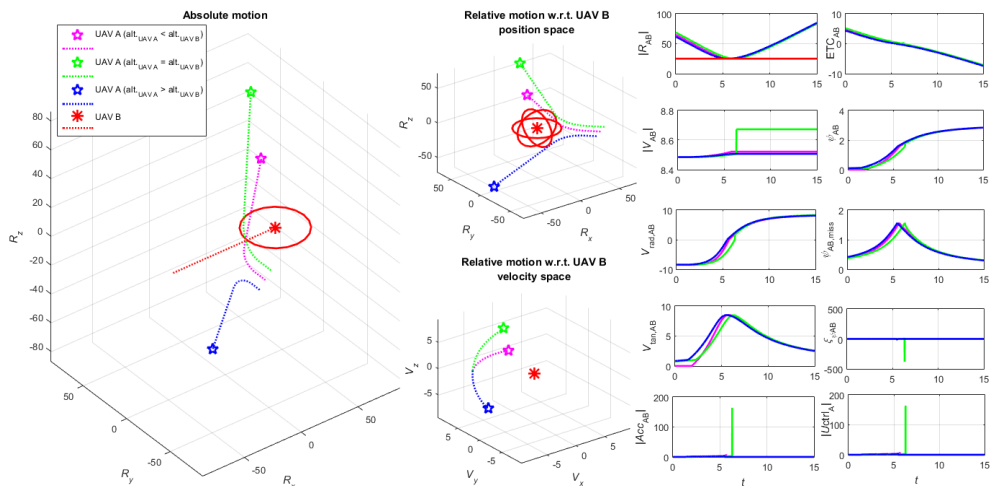


Figure 41. CA maneuver with various initial position (3D)
Case #4 (magenta), Case #5 (green), & Case #6 (blue)

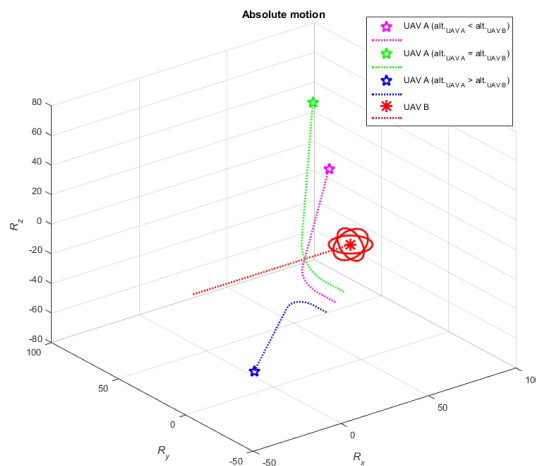


Figure 42. Position evolution of both UAVs in global perspective
Case #4 (magenta), Case #5 (green), & Case #6 (blue)

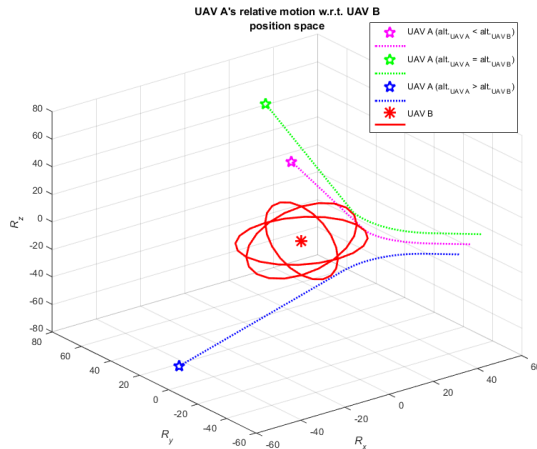


Figure 43. Position evolution of UAV A relative to UAV B in Case #4 (magenta), Case #5 (green), & Case #6 (blue)

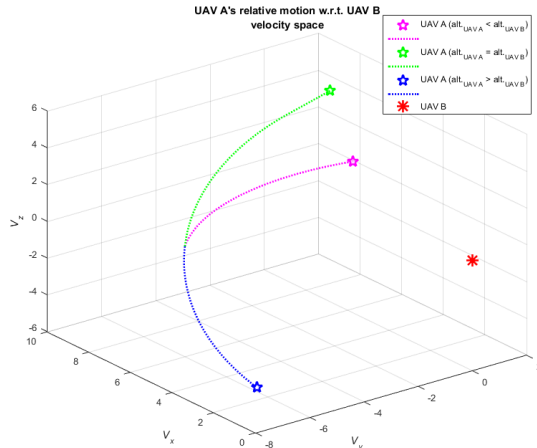


Figure 44. Velocity evolution of UAV A relative to UAV B in Case #4 (magenta), Case #5 (green), & Case #6 (blue)

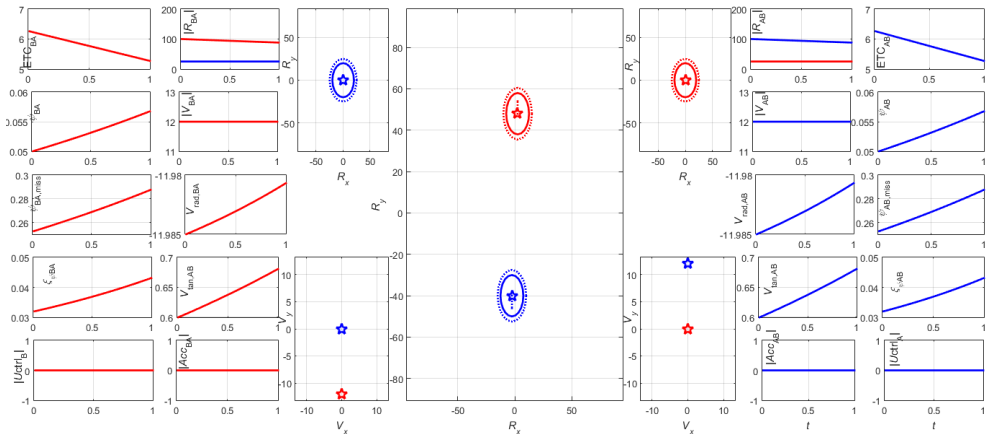


Figure 45. Front encounter: Initial condition

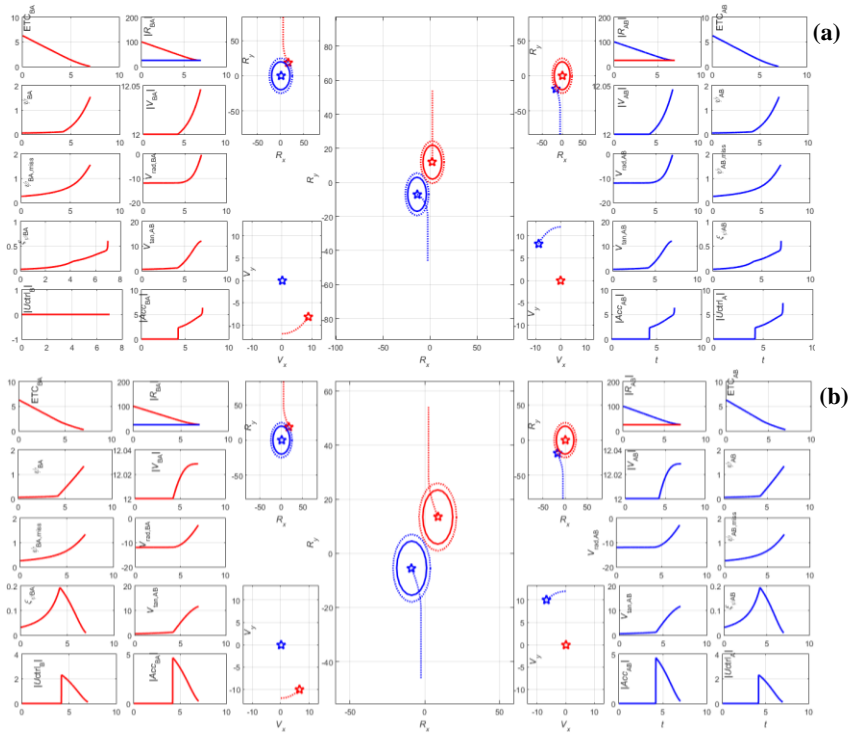


Figure 46. Front encounter: at closest separation
 (a) non-cooperative CA, (b) cooperative CA

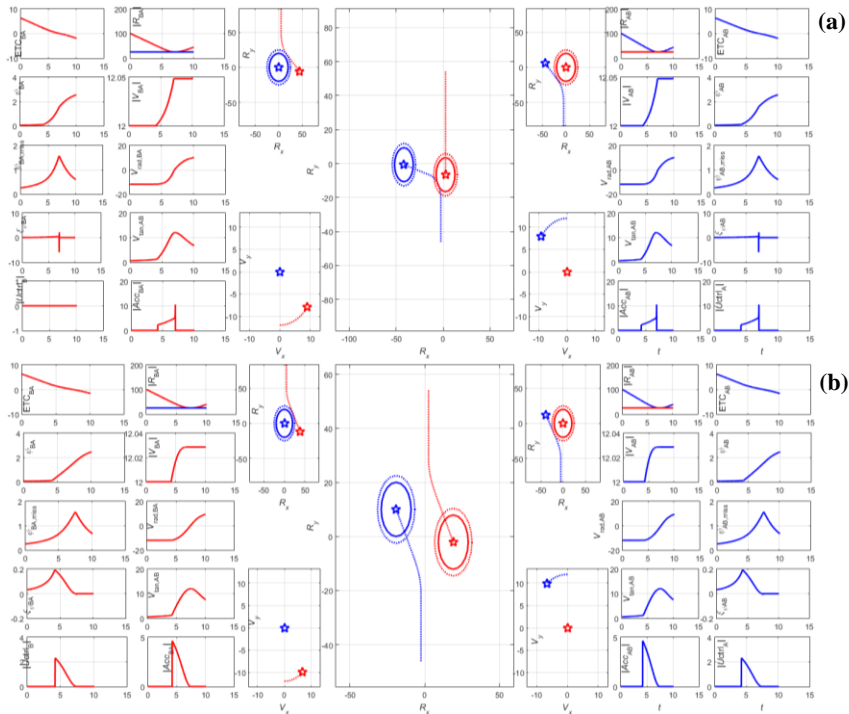


Figure 47. Front encounter: after successfully avoiding collision
 (a) non-cooperative CA, (b) cooperative CA

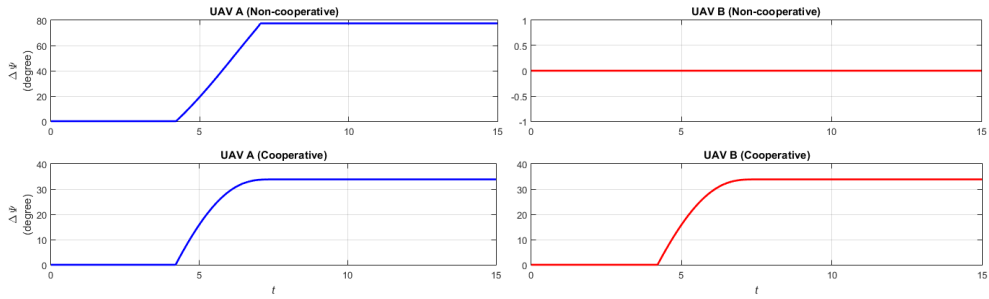


Figure 48. Front Encounter: Trajectory Deflection

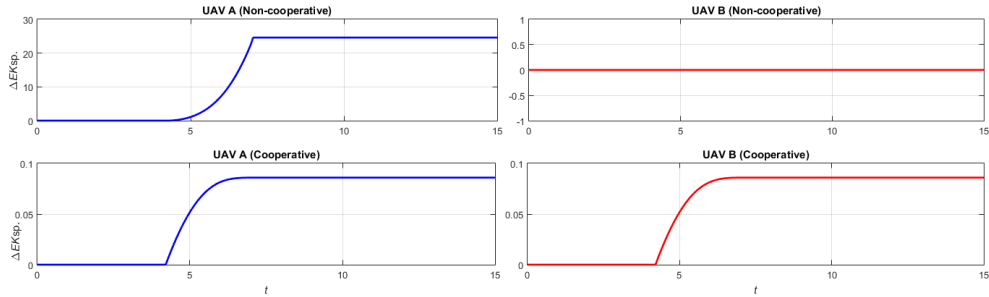


Figure 49. Front Encounter: Specific Kinetic Energy Change

B.3. Non-cooperative CA v.s. Cooperative CA

Initial condition is set to create a collision threat situation from a front encounter event. As can be seen sequentially in Figure 45, Figure 46(a), and Figure 47(a), the working CA controller is only on UAV A; collision avoidance on both UAVs is non-cooperative. UAV A’s trajectory is deflected to about 77.5° with respect to its initial direction while UAV B maintains its initial direction (Figure 47(a) & Figure 48). In the sequence Figure 45-Figure 46(b)-Figure 47(b), CA controller is working on both UAVs; collision avoidance is cooperative. Trajectory deflection is only 33.8° for each UAV since both UAVs use the same value for their respective CA controller gain (Figure 47(b) & Figure 48). One can expect the trajectory deflection on each UAV to differ if the gain value on both UAV are not equal. Meanwhile, results in Figure 49 shows that cooperative CA behavior significantly reduce the amount of kinetic energy change to perform successful CA.

4. Conclusion

A collision avoidance (CA) control system that is based on collision threat situation (CTS) model is presented. We construct our model using kinematic relations between motion variables of a pair of UAVs under a collision threat situation (CTS). We also identify the parameters that play essential role in CTS. From these parameters, we define the state variable of the collision threat system by which a CTS may be quantified. The CA controller is formulated based on the quantification so that it acts to reduce the value of the threat state variable. We analyze the stability of our CA control system using threat system’s energy evaluation. The analysis provides us useful relations between system’s stability with some constraints achievable by CA control system, angularly and translationally.

From the stability analysis and results on the simulated test cases, the resulting CA control system has shown its capability to work on a three-dimensional cases. It can be applied to a one-on-one CA control system as non-cooperative control scheme, as well as cooperative control scheme. CTS with multiple intruders can be dealt with by assigning priority to intruder that presents the greatest threat according to the threat state equation (29).

Our relative-motion kinematic-based CTS model is advantageous in determining the shortest evasive trajectory for the evading vehicle that can be inferred sufficiently by the two vectors: the vector of relative distance, and the vector of relative velocity. These two vectors are obtainable by appropriate measuring technique using laser-based range-and-directional sensors. We design our collision avoidance controller by exploiting this advantage. Obtaining these two measures is sufficient to define the collision threat state using (29) and is also sufficient to determine which evasion plane that must be taken by the evading vehicle. This reduces the number of possible evasion plane that must be evaluated from infinity to one, thus eliminating the need to perform a search-based solution optimization.

Lastly, in designing the CA controller, we do not consider coupling the CA task with a goal-tracking task to recover the controlled vehicle initial heading. If we consider any typical avoid-and-recover scenario, the CA task and the goal-tracking task are executed consecutively (tracking-CA-tracking), not simultaneously. Control system that executes both tasks simultaneously is problematic since a goal-tracking action may oppose the collision avoidance action, and vice versa. The CA controller in such condition is ineffective and put the controlled vehicle at risk of collision. Also, when CA and goal-tracking are coupled, it would be difficult to evaluate the performance of either controller.

5. References

- [1] Khatib, Oussama, “Real-Time Obstacle Avoidance for Manipulators and Mobile Robots”, *The International Journal of Robotics Research*, vol. 5(1), 1986, pp. 90-98.
- [2] Mastellone, Silvia; Stipanovic, Dusan M.; Graunke, Christopher R.; Intlekofer, Koji A.; Spong, Mark W.; “Formation Control and Collision Avoidance for Multi-Agent Non-Holonomic Systems: Theory and Experiments”, *The International Journal of Robotics Research*, vol. 27, 2008, pp. 107-126. DOI: [10.1177/0278364907084441](https://doi.org/10.1177/0278364907084441)
- [3] Yan, Jin; Guan, Xin-Ping; Luo, Xiao-Yuan; Tan, Fu-Xiao; “Target Tracking and Obstacle Avoidance for Multi-Agent Networks with Input Constraints”, *International Journal of Automation and Computing*, vol. 8(1), 2011, pp. 46-53. DOI: [10.1007/s11633-010-0553-1](https://doi.org/10.1007/s11633-010-0553-1)
- [4] Listmann, Kim D.; Masalawala, Mohanish V.; Adamy, Jürgen; “Consensus for Formation Control of Nonholonomic Mobile Robots”, *IEEE International Conference on Robotics and Automation*, 2009, pp.3886-3891. DOI: [10.1109/ROBOT.2009.5152865](https://doi.org/10.1109/ROBOT.2009.5152865)
- [5] Chang, Dong Eui; Marsden, Jerrold E.; “Gyroscopic Forces and Collision Avoidance with Convex Obstacles” chapter in “New Trends in Nonlinear Dynamics and Control, and Their Applications”, 2003, Editors: Kang, Wei; Borges, Carlos; Xiao, Mingqing. DOI: [10.1007/978-3-540-45056-6_9](https://doi.org/10.1007/978-3-540-45056-6_9)
- [6] Chang, Dong Eui; Shadden, Shawn C.; Marsden, Jerrold E.; Olfati-Saber, Reza; “Collision Avoidance for Multiple Agent Systems”, in *Proceedings of the 42nd IEEE Conference on Decision and Control*, Maui, Hawaii USA, 2003. DOI: [10.1109/CDC.2003.1272619](https://doi.org/10.1109/CDC.2003.1272619)
- [7] Kobilarov, Marin; “Gyroscopic Obstacle Avoidance in 3D”, ASCO Lab Technical notes, Johns Hopkins University. Available online at https://asco.lcsr.jhu.edu/papers/Ko2013_gyro.pdf, accessed on Dec 8, 2015.
- [8] Chakravarthy, A.; Ghose, D.; “Obstacle Avoidance in A Dynamic Environment: A Collision Cone Approach”, *IEEE Trans. on Systems, Man, and Cybernetics –Part A: Systems and Humans*, Vol. 28(5), 1998.
- [9] Paolo Fiorini, & Zvi Shiller, “Motion Planning in Dynamic Environments using Velocity Obstacles”, *The International Journal of Robotics Research*, vol. 17(7), 1998, pp. 760-772. DOI: [10.1177/027836499801700706](https://doi.org/10.1177/027836499801700706)
- [10] Berg, Jur v.d.; Lin, Ming; Manocha, Dinesh; “Reciprocal Velocity Obstacles for Real-Time Multi-Agent Navigation”, in *proc. of the IEEE International Conference on Robotics and Automation* 2008.
- [11] Berg, Jur v.d.; Guy, Stephen J.; Lin, Ming; Manocha, Dinesh; “Reciprocal n -Body Collision Avoidance”, *The 14th International Symposium of Robotics Research*, 2011, pp. 3-19. DOI: [10.1007/978-3-642-19457-3_1](https://doi.org/10.1007/978-3-642-19457-3_1)

- [12] Jenie, Y. I.; Kampen, E. J.; Visser, C. C.; Ellerbroek, J.; Hoekstra, J. M.; “Three-Dimensional Velocity Obstacle Method for Uncoordinated Avoidance Maneuvers of Unmanned Aerial Vehicles”, *AIAA Journal of Guidance, Control, and Dynamics*, vol. 39, no. 10, pp. 2312-2323, 2016. DOI: [10.2514/1.G001715](https://doi.org/10.2514/1.G001715)
- [13] Orlando, V.A.; Welch, J.D.; “Beacon CAS (BCAS): An Integrated Air/Ground Collision Avoidance System”, *Federal Aviation Administration*, 1976.
- [14] Kochenderfer, Mykel J.; Espindle, Leo P.; Griffith, J. Daniel; Kuchar, James K.; “A Bayesian Approach to Aircraft Encounter Modeling”, *AIAA Guidance, Navigation and Control Conference and Exhibit*, 2008, DOI: [10.2514/6.2008-6629](https://doi.org/10.2514/6.2008-6629)
- [15] Kochenderfer, Mykel J.; Espindle, Leo P.; Griffith, J. Daniel; Kuchar, James K.; “Encounter Modeling for Sense and Avoid Development”, *Integrated Communications, Navigation and Surveillance Conference*, 2008. DOI: [10.1109/ICNSURV.2008.4559177](https://doi.org/10.1109/ICNSURV.2008.4559177)
- [16] Kochenderfer, Mykel J.; Espindle, Leo P.; Kuchar, James K.; Griffith, J. Daniel; “A Comprehensive Aircraft Encounter Model of The National Airspace System”, *Lincoln Laboratory Journal*, vol. 17, no. 2, 2008. DOI: [10.1.1.161.4070](https://doi.org/10.1.1.161.4070)
- [17] Kochenderfer, Mykel J.; Edwards, Matthew W.M.; Espindle, Leo P.; Kuchar, James K.; Griffith, J. Daniel; “Airspace Encounter Models for Estimating Collision Risk”, *AIAA Journal of Guidance, Control, and Dynamics*, vol. 33, no. 2, pp. 487-499, 2010. DOI: [10.2514/1.44867](https://doi.org/10.2514/1.44867)
- [18] Kochenderfer, Mykel J.; Holland, Jessica E.; Chryssanthacopoulos, James P.; “Next-Generation Airborne Collision Avoidance System”, *Lincoln Laboratory Journal*, vol. 19, no. 1, 2012.



Tata Sudiyanto is a PhD student at the School of Electrical Engineering and Informatics ITB (STEI-ITB), Indonesia. He received his Master degree of Aeronautics and Astronautics in 2010 from the Faculty of Aerospace and Mechanical Engineering ITB (FTMD-ITB), Indonesia, and his Bachelor degree of Aeronautics and Astronautics in 2005 from the Department of Aeronautics and Astronautics Engineering, formerly of the Faculty of Industrial Technology ITB (FTI-ITB). He works for PT Parametrik Solusi Integrasi, an engineering company, as a computer-aided analysis (CAA) engineer.



Bambang Riyanto Trilaksono was born in Banyuwangi, Indonesia in 1962. He obtained his undergraduate degree from Electrical Engineering in Bandung Institute of Technology in 1986. He obtained his master and PhD degree from Electrical Engineering, Waseda University, Japan, in 1991 and 1994, respectively. Currently, he is a professor in Control and Computer System Research Group in Bandung Institute of Technology. His research interests include control, robotics and artificial intelligence.



Agus Budiyo is a scientist and a technopreneur who received four degrees in Aeronautics and Astronautics including Master's and Engineer's degrees from MIT. He is author of 200+ papers and several books leading to startups activities in the US, South Korea, and Indonesia. He co-founded the Center of Unmanned System Studies at ITB as the precursor of national defense industry. He is the Director of R&D at Parametrik Solusi Integrasi since 2012. He is also the Director of R&D at Bhimasena Research and Development.



Widyardana Adiprawita, lecturer at STEI-ITB. Received his electrical engineering degree at Electrical Engineering ITB with honour in 1997. Finished master degree at Informatics Engineering ITB in 2000. He finished his doctoral degree with honour at Electrical Engineering ITB. His Research interests are embedded system, robotics and intelligent agent autonomy. He has written more than 20 papers published in international and national publication.